The Eshelby Tensors in a Finite Spherical Domain—Part II: Applications to Homogenization

Shaofan Li[1]
e-mail: li@ce.berkeley.edu

Gang Wang

Roger A. Sauer

Department of Civil and Environmental Engineering,
University of California,
Berkeley, CA 94720

In this part of the work, the Eshelby tensors of a finite spherical domain are applied to various homogenization procedures estimating the effective material properties of multiphase composites. The Eshelby tensors of a finite domain can capture the boundary effect of a representative volume element as well as the size effect of the different phases. Therefore their application to homogenization does not only improve the accuracy of classical homogenization methods, but also leads to some novel homogenization theories. This paper highlights a few of them: a refined dilute suspension method and a modified Mori–Tanaka method, the exterior eigenstrain method, the dual-eigenstrain method, which is a generalized self-consistency method, a shell model, and new variational bounds depending on the different boundary conditions. To the best of the authors' knowledge, this is the first time that a multishell model is used to evaluate the Hashin–Shtrikman bounds for a multiple phase composite ($n \geqslant 3$)*, which can distinguish some of the subtleties of different microstructures.* [DOI: 10.1115/1.2711228]

1 Introduction

In the first part of this work [1], which is referred to as Part I hereafter, the exact solutions of the elastic fields of a spherical inclusion embedded in a finite spherical representative volume (RVE) are obtained under both the prescribed displacement (Dirichlet) boundary condition and the prescribed traction (Neumann) boundary condition.

For simplicity, we refer to the Dirichlet– and Neumann–Eshelby tensors of a finite domain as the finite Eshelby tensors. A salient feature of the finite Eshelby tensors is their ability to capture both the boundary effect, or image force effect, of an RVE and the size effect, i.e., the dependency on the volume fraction of the different phases of a composite. This offers great advantages and flexibilities in homogenization procedures, which is the focus of this second part of our work. Using the new finite Eshelby tensors we can modify the classical homogenization schemes and obtain some remarkable results. Furthermore several new homogenization schemes can be constructed by the application of the finite Eshelby tensors.

In recent years, nanocomposites have emerged as promising materials for future technologies e.g., Refs. [2,3], because of their high strength, excellent conductivity in both heat transfer and electricity. Considerable attention has been devoted to study the interfacial strength, size effects, and agglomeration effects of nanocomposites (e.g. Fisher et al. [4], Odegard et al. [5], Shi et al. [6], and Sharma and Ganti [7]). The classical homogenization techniques have shown limitations to deal with the above issues. There is a call for a refined micromechanics theory for nanocomposites, e.g, Ref. [8]. One of the objectives of this research is towards establishing a refined micromechanics homogenization theory for nanocomposites.

We proceed, in the following section, by deriving expressions for the average finite Eshelby tensors in a RVE. These are needed to characterize the average disturbance fields, which have some important properties. In Sec. 3 we re-examine two conventional homogenization methods by using the average finite Eshelby tensor. Further, in Sec. 4, we discuss the so-called dual eigenstrain method, which is a combination of an exterior and interior eigenstrain homogenization method. This scheme is a generalized self-consistency method, which leads to a new class of predictor–corrector schemes. In Sec. 5, a shell model is proposed to capture microstructure effects on the homogenization of a multiphase composite. Finally, in Sec. 6, the Hashin–Shtrikman (HS) variational bounds are rederived using the finite Eshelby tensors to incorporate the boundary conditions. A multishell model is used to evaluate the exact HS bounds for a multiphase composite with $n \geqslant 3$ using a multivariable optimization procedure. Conclusions are drawn in Sec. 7.

2 Average Eshelby Tensors and Average Disturbance Fields

In Part I we derived the finite Eshelby tensors, $\mathbb{S}^{\cdot,D}$ and $\mathbb{S}^{\cdot,N}$, which are valid for a spherical inclusion Ω_I embedded at the center of a finite, spherical RVE Ω (see Fig. 1 of Part I). In accordance with Part I we adopt the following nomenclature to describe the problem: The radii of inclusion and RVE are denoted by a and A, their ratio by $\rho_0 = a/A$. Any point $\mathbf{x}$ inside the RVE can be written as $\mathbf{x} = tA\bar{\mathbf{x}}$, where $t = |\mathbf{x}|/A$ and $\bar{\mathbf{x}} = \mathbf{x}/|\mathbf{x}|$ denote the normalized radial distance and direction of $\mathbf{x}$. The elasticity tensors of the two domains Ω_I and Ω_E are denoted by $\mathbb{C}^I$ and $\mathbb{C}^E = \mathbb{C}$.

For clarity, we first derive the expression of the average finite Eshelby tensors and discuss their relation with the average disturbance strain field.

2.1 Average Eshelby Tensors. The spatial averaging operator is defined as

$$\langle \dots \rangle_\Omega = \frac{1}{|\Omega|} \int_\Omega \dots d\Omega \tag{1}$$

where $|\Omega|$ denotes the volume of the spatial domain Ω. Due to the radial isotropic structure of the finite Eshelby tensors, $\mathbb{S}^{\star}_{ijmn}(\mathbf{x}) = \mathbf{\Theta}^T_{ijmn}(\bar{\mathbf{x}})\mathbf{S}^{\cdot,\star}(t)$ ($\cdot = I, E$; $\star = D, N$), their average over the RVE domain Ω can be written as

[1]Corresponding author.

Contributed by the Applied Mechanics Division of ASME for publication in the JOURNAL OF APPLIED MECHANICS. Manuscript received April 6, 2006; final manuscript received June 14, 2006. Review conducted by Subrata Mukherjee. Paper presented at the 2005 ASME International Mechanical Engineering Congress (IMECE2005), Orlando, FL, USA, November 5–11, 2005.

$$\langle \mathbb{S}^{\cdot,\star}_{ijmn}(\mathbf{x})\rangle_\Omega = \frac{1}{|\Omega|}\int_\Omega \mathbf{S}^{\cdot,\star}(t)\cdot\boldsymbol{\Theta}_{ijmn}(\bar{\mathbf{x}})d\Omega = \langle 3t^2\mathbf{S}^{\cdot,\star}\rangle_{[0,1]}\cdot\langle\boldsymbol{\Theta}_{ijmn}\rangle_{S_2} \tag{2}$$

where S_2 denotes the surface of a sphere with unit radius, and where

$$\langle\boldsymbol{\Theta}_{ijmn}\rangle_{S_2} := \frac{1}{4\pi}\int_{S_2}\boldsymbol{\Theta}_{ijmn}\,dS_2 \tag{3}$$

$$\langle 3t^2\mathbf{S}^{\cdot,\star}\rangle_{[a,b]} := \frac{1}{b^3-a^3}\int_a^b 3t^2\mathbf{S}^{\cdot,\star}\,dt \tag{4}$$

The above decomposition is possible since $\mathbf{S}$ is independent of the orientation $\bar{\mathbf{x}}$ and $\boldsymbol{\Theta}_{ijmn}$ is independent of the radial distance t. Performing the averaging of $\boldsymbol{\Theta}_{ijmn}$ over the unit sphere yields

$$\langle\boldsymbol{\Theta}_{ijmn}\rangle_{S_2} = \frac{1}{4\pi}\int_{S_2}\boldsymbol{\Theta}_{ijmn}\,dS_2 = \begin{bmatrix} 3\mathbb{E}^{(1)}_{ijmn} \\ 2\mathbb{E}^{(1)}_{ijmn}+2\mathbb{E}^{(2)}_{ijmn} \\ \mathbb{E}^{(1)}_{ijmn} \\ \mathbb{E}^{(1)}_{ijmn} \\ \frac{4}{3}\mathbb{E}^{(1)}_{ijmn}+\frac{4}{3}\mathbb{E}^{(2)}_{ijmn} \\ \frac{1}{3}\mathbb{E}^{(1)}_{ijmn}+\frac{2}{15}\mathbb{E}^{(2)}_{ijmn} \end{bmatrix} = \begin{bmatrix} 3 & 0 \\ 2 & 2 \\ 1 & 0 \\ 1 & 0 \\ \frac{4}{3} & \frac{4}{3} \\ \frac{1}{3} & \frac{2}{15} \end{bmatrix} \times \begin{bmatrix} \mathbb{E}^{(1)}_{ijmn} \\ \mathbb{E}^{(2)}_{ijmn} \end{bmatrix} \tag{5}$$

where $\mathbb{E}^{(1)}_{ijmn}$ and $\mathbb{E}^{(2)}_{ijmn}$ are the following isotropic basis tensors

$$\mathbb{E}^{(1)}_{ijmn} = \tfrac{1}{3}\delta_{ij}\delta_{mn}, \quad \mathbb{E}^{(2)}_{ijmn} = \tfrac{1}{2}(\delta_{im}\delta_{jn}+\delta_{in}\delta_{jm}) - \tfrac{1}{3}\delta_{ij}\delta_{mn} \tag{6}$$

For each boundary condition (Dirichlet or Neumann), we have two Eshelby tensors, interior $\mathbb{S}^{I,\star}(\mathbf{x})$ for $\mathbf{x}\in\Omega_I$, or exterior $\mathbb{S}^{E,\star}(\mathbf{x})$ for $\mathbf{x}\in\Omega/\Omega_I := \Omega_E$. Their average over the respective domains follows as

$$\langle \mathbb{S}^{I,\star}_{ijmn}\rangle_{\Omega_I} = \langle 3t^2\mathbf{S}^I\rangle_{[0,\rho_0]}\cdot\langle\boldsymbol{\Theta}_{ijmn}\rangle_{S_2},$$

$$\langle \mathbb{S}^{E,\star}_{ijmn}\rangle_{\Omega_E} = \langle 3t^2\mathbf{S}^E\rangle_{[\rho_0,1]}\cdot\langle\boldsymbol{\Theta}_{ijmn}\rangle_{S_2} \tag{7}$$

Since the averaging of $\boldsymbol{\Theta}_{ijmn}$ over S_2 is an isotropic tensor, we obtain

$$\langle \mathbb{S}^{I,\star}_{ijmn}\rangle_{\Omega_I} = s_1^{I,\star}\mathbb{E}^{(1)}_{ijmn} + s_2^{I,\star}\mathbb{E}^{(2)}_{ijmn} \tag{8}$$

$$\langle \mathbb{S}^{E,\star}_{ijmn}\rangle_{\Omega_E} = s_1^{E,\star}\mathbb{E}^{(1)}_{ijmn} + s_2^{E,\star}\mathbb{E}^{(2)}_{ijmn} \tag{9}$$

The coefficients $s_1^{I,\star}$, $s_2^{I,\star}$ and $s_1^{E,\star}$, $s_2^{E,\star}$ depend on the volume fraction $f := \rho_0^3$ and are given as

$$s_1^{I,D} = \frac{(1+\nu)(1-f)}{3(1-\nu)}, \quad s_2^{I,D} = \frac{2(4-5\nu)(1-f)}{15(1-\nu)} - 21\gamma_u[f](1-f^{2/3}) \tag{10}$$

$$s_1^{E,D} = -\frac{(1+\nu)f}{3(1-\nu)}, \quad s_2^{E,D} = -\frac{2(4-5\nu)f}{15(1-\nu)} + 21\gamma_u[f]f\frac{1-f^{2/3}}{1-f} \tag{11}$$

for the Dirichlet boundary condition (BC) and

$$s_1^{I,N} = \frac{1+\nu+2(1-2\nu)f}{3(1-\nu)},$$

$$s_2^{I,N} = \frac{2(4-5\nu)+(7-5\nu)f}{15(1-\nu)} + 21\gamma_l[f](1-f^{2/3}) \tag{12}$$

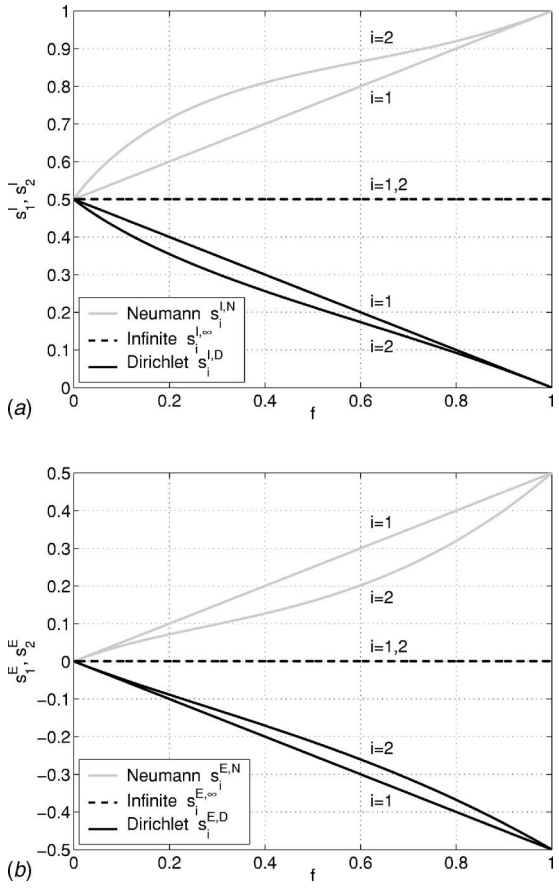

Fig. 1 Average Eshelby tensor coefficients s_1^I, s_1^E ($i=1$) and s_2^I, s_2^E ($i=2$)

$$s_1^{E,N} = \frac{2(1-2\nu)f}{3(1-\nu)}, \quad s_2^{E,N} = \frac{(7-5\nu)f}{15(1-\nu)} - 21\gamma_l[f]f\frac{1-f^{2/3}}{1-f} \tag{13}$$

for the Neumann BC. Here we have denoted

$$\gamma_u[f] := \frac{f(1-f^{2/3})}{10(1-\nu)(7-10\nu)}, \quad \gamma_l[f] := \frac{4f(1-f^{2/3})}{10(1-\nu)(7+5\nu)} \tag{14}$$

In fact, Eqs. (10)–(13) are the precise formulas of the size-effect characterization of of the inclusion problem. One can find that this effect is linear for the bulk modulus, whereas it is nonlinear in the shear modulus. In contrast to the average finite Eshelby tensors we recall the average Eshelby tensor for a spherical inclusion in an unbounded medium

$$\langle \mathbb{S}^{\cdot,\infty}_{ijmn}\rangle_{\Omega_\cdot} = s_1^{\cdot,\infty}\mathbb{E}^{(1)}_{ijmn} + s_2^{\cdot,\infty}\mathbb{E}^{(2)}_{ijmn}, \quad \cdot = I \text{ or } E \tag{15}$$

$$s_1^{I,\infty} = \frac{1+\nu}{3(1-\nu)}, \quad s_2^{I,\infty} = \frac{2(4-5\nu)}{15(1-\nu)} \tag{16}$$

$$s_1^{E,\infty} = 0, \quad s_2^{E,\infty} = 0 \tag{17}$$

Figure 1 displays the behaviors of all the coefficients $s_i^{\cdot,\star}$ in dependence of f. The Poisson's ratio is chosen as $\nu=0.2$. We observe that for the Dirichlet case the coefficients decrease, while for the Neumann case they increase with growing f. The classical Eshelby tensors do not depend on f.

Note that when $f\to 0$ in Eqs. (10)–(13) we recover the expressions for the average of the classical Eshelby tensors. The fact that $s_i^{E,\infty}=0$ implies the well-known Tanaka–Mori Lemma (see below). Let us define the difference $\Delta s_i^\star = s_i^{I,\star} - s_i^{E,\star}$; we have

$$\Delta s_1^D = \Delta s_1^N = \Delta s_1^\infty = \frac{1+\nu}{3(1-\nu)} \tag{18}$$

$$\Delta s_2^D = \Delta s_2^\infty - 21\gamma_u[f]\frac{1-f^{2/3}}{1-f}, \quad \Delta s_2^\infty = \frac{2(4-5\nu)}{15(1-\nu)} \tag{19}$$

$$\Delta s_2^N = \Delta s_2^\infty + 21\gamma_t[f]\frac{1-f^{2/3}}{1-f} \tag{20}$$

2.2 The Average Disturbance Fields. The finite Eshelby tensors can be conveniently used to represent the average disturbance fields. Recall the classical Tanaka–Mori Lemma [9]: the exterior average disturbance strain in the exterior domain is zero (see Eq. (17))

$$\langle \boldsymbol{\epsilon}^d \rangle_{\Omega_E} = \langle \mathbb{S}^{E,\infty} \rangle_{\Omega_E} : \boldsymbol{\epsilon}^* = (s_1^{E,\infty}\mathbb{E}^{(1)} + s_2^{E,\infty}\mathbb{E}^{(2)}) : \boldsymbol{\epsilon}^* = 0 \tag{21}$$

A similar result holds for the disturbance stress field for a linear elastic medium. Using the new finite Eshelby tensors $\mathbb{S}^D$ and $\mathbb{S}^N$ the original Tanaka–Mori Lemma result is modified. The exterior average disturbance strain field is neither zero for the Dirichlet problem

$$\langle \boldsymbol{\epsilon}^d \rangle_{\Omega_E} = \langle \mathbb{S}^{E,D} \rangle_{\Omega_E} : \boldsymbol{\epsilon}^* = (s_1^{E,D}\mathbb{E}^{(1)} + s_2^{E,D}\mathbb{E}^{(2)}) : \boldsymbol{\epsilon}^* \neq 0 \tag{22}$$

nor is it zero for the Neumann problem

$$\langle \boldsymbol{\epsilon}^d \rangle_{\Omega_E} = \langle \mathbb{S}^{E,N} \rangle_{\Omega_E} : \boldsymbol{\epsilon}^* = (s_1^{E,N}\mathbb{E}^{(1)} + s_2^{E,N}\mathbb{E}^{(2)}) : \boldsymbol{\epsilon}^* \neq 0 \tag{23}$$

(unless $f=0$). However, in view of Eqs. (11) and (13), we find that for both problems

$$\langle \boldsymbol{\epsilon}^d \rangle_{\Omega_E} = \mathcal{O}(f) \tag{24}$$

which can be viewed as a modified Tanaka–Mori Lemma. One then recovers the original result as $f \to 0$.

Moreover, consider the Dirichlet problem. We can exactly satisfy a key assumption, the average strain theorem

$$\langle \boldsymbol{\epsilon} \rangle_\Omega = \langle \boldsymbol{\epsilon}^0 + \boldsymbol{\epsilon}^d \rangle_\Omega = \boldsymbol{\epsilon}^0 + \langle \boldsymbol{\epsilon}^d \rangle_\Omega = \boldsymbol{\epsilon}^0 \tag{25}$$

since the average disturbance strain field in Ω is zero

$$\langle \boldsymbol{\epsilon}^d \rangle_\Omega = f\langle \boldsymbol{\epsilon}^d \rangle_{\Omega_I} + (1-f)\langle \boldsymbol{\epsilon}^d \rangle_{\Omega_E} = [f\langle \mathbb{S}^{I,D} \rangle_{\Omega_I} + (1-f)\langle \mathbb{S}^{E,D} \rangle_{\Omega_E}] : \boldsymbol{\epsilon}^* = 0 \tag{26}$$

Likewise, for the Neumann problem, the average stress theorem

$$\langle \boldsymbol{\sigma} \rangle_\Omega = \boldsymbol{\sigma}^0 \tag{27}$$

is exactly satisfied since $\langle \boldsymbol{\sigma}^d \rangle_\Omega = f\langle \boldsymbol{\sigma}^d \rangle_{\Omega_I} + (1-f)\langle \boldsymbol{\sigma}^d \rangle_{\Omega_E} = 0$ due to

$$f\langle \mathbb{T}^{I,N} \rangle_{\Omega_I} + (1-f)\langle \mathbb{T}^{E,N} \rangle_{\Omega_E} = \mathbb{O} \tag{28}$$

where $\mathbb{T}^{I,N}$ and $\mathbb{T}^{E,N}$ are the conjugate Neumann Eshelby tensors related to the Neumann Eshelby tensors by the expressions

$$\langle \mathbb{S}^{I,N} \rangle_{\Omega_I} + \langle \mathbb{T}^{I,N} \rangle_{\Omega_I} = \mathbb{I}^s$$

and

$$\langle \mathbb{S}^{E,N} \rangle_{\Omega_E} + \langle \mathbb{T}^{E,N} \rangle_{\Omega_E} = \mathbb{O} \tag{29}$$

where $\mathbb{I}^s$ is the fourth-order symmetric unit tensor and $\mathbb{O}$ is the fourth-order null tensor.

3 Improvement of the Classical Homogenization Methods

We now use the finite Eshelby tensors in two classical homogenization procedures to estimate effective material properties, namely, the homogenization for composites with dilute suspension and the Mori–Tanaka model.

3.1 Dilute Suspension Model. The dilute suspension method predicts two different effective elastic tensors depending on the different boundary conditions e.g., Ref. [10]. We first consider the prescribed macrostrain BC, i.e., the Dirichlet boundary value problem (BVP) ($\mathbf{u}^d = 0$ on $\partial\Omega$), as discussed in Part I. The average stress consistency condition for the considered homogenization scheme (for prescribed eigenstrain within Ω_I as motivated in Part I) is

$$\mathbb{C}^I : (\boldsymbol{\epsilon}^0 + \langle \boldsymbol{\epsilon}^d \rangle_{\Omega_I}) = \mathbb{C} : (\boldsymbol{\epsilon}^0 + \langle \boldsymbol{\epsilon}^d \rangle_{\Omega_I} - \boldsymbol{\epsilon}^*), \quad \forall \in \Omega_I \tag{30}$$

Note that $\mathbb{C}^I$, $\mathbb{C}$, $\boldsymbol{\epsilon}^0$, and $\boldsymbol{\epsilon}^*$ are considered constant. From Eq. (30) we obtain

$$\boldsymbol{\epsilon}^0 + \langle \boldsymbol{\epsilon}^d \rangle_{\Omega_I} = \mathbb{A} : \boldsymbol{\epsilon}^* \tag{31}$$

where $\mathbb{A} := (\mathbb{C} - \mathbb{C}^I)^{-1} : \mathbb{C}$. Consider the interior average of the disturbance strain field

$$\langle \boldsymbol{\epsilon}^d \rangle_{\Omega_I} = \langle \mathbb{S}^{I,D} \rangle_{\Omega_I} : \boldsymbol{\epsilon}^* \tag{32}$$

and substitute Eq. (32) into Eq. (31). This yields

$$\boldsymbol{\epsilon}^* = [\mathbb{A} - \langle \mathbb{S}^{I,D} \rangle_{\Omega_I}]^{-1} : \boldsymbol{\epsilon}^0 \tag{33}$$

and consequently,

$$\langle \boldsymbol{\epsilon} \rangle_{\Omega_I} = \boldsymbol{\epsilon}^0 + \langle \boldsymbol{\epsilon}^d \rangle_{\Omega_I} = \mathbb{A} : [\mathbb{A} - \langle \mathbb{S}^{I,D} \rangle_{\Omega_I}]^{-1} : \boldsymbol{\epsilon}^0 \tag{34}$$

Following the standard procedure, e.g., Ref. [10], we find the estimate of the effective elasticity tensor for the prescribed macrostrain BC

$$\bar{\mathbb{C}} = \mathbb{C} - f\mathbb{C} : (\mathbb{A} - \langle \mathbb{S}^{I,D} \rangle_{\Omega_I})^{-1} \tag{35}$$

The only difference between Eq. (35) and the classical solution for dilute suspension is that a different Eshelby tensor is used. Considering isotropic materials, the effective bulk and shear moduli become

$$\bar{\kappa} = \kappa - f\kappa\left(\frac{1}{1-\kappa^I/\kappa} - s_1^{I,D}\right)^{-1}, \quad \bar{\mu} = \mu - f\mu\left(\frac{1}{1-\mu^I/\mu} - s_2^{I,D}\right)^{-1} \tag{36}$$

For the prescribed macrostress boundary condition, the new dilute suspension estimate is

$$\bar{\mathbb{D}} = \mathbb{D} + f\mathbb{D} : (\mathbb{A} - \langle \mathbb{S}^{I,N} \rangle_{\Omega_I})^{-1} \tag{37}$$

where $\langle \mathbb{S}^{I,N} \rangle_{\Omega_I}$ is the interior average Neumann–Eshelby tensor. For isotropic composites, the corresponding effective bulk and shear moduli are

$$\bar{\kappa}^{-1} = \kappa^{-1} + f\kappa^{-1}\left(\frac{1}{1-\kappa^I/\kappa} - s_1^{I,N}\right)^{-1},$$

$$\bar{\mu}^{-1} = \mu^{-1} + f\mu^{-1}\left(\frac{1}{1-\mu^I/\mu} - s_2^{I,N}\right)^{-1} \tag{38}$$

Figure 2 shows the curves of the normalized bulk modulus, $\bar{\kappa}/\kappa$, and shear modulus, $\bar{\mu}/\mu$, in dependence of the volume fraction f of the inclusion. The material properties of the inclusion are chosen as $\kappa^I/\kappa = 10$, $\mu^I/\mu = 4$, with $\nu = 0.1$. We have plotted the result Eq. (35) using the Dirichlet–Eshelby tensor $\mathbb{S}^{I,D}$ (dark) and (37) using the Neumann–Eshelby tensor $\mathbb{S}^{I,N}$ (light). We compare the new results with the conventional dilute suspension results using the infinite Eshelby tensor $\mathbb{S}^{I,\infty}$ in Eq. (35) (dashed line 2) and in Eq. (37) (dashed line 1).

From this figure, we can observe the well-known result that the classical solution is not self-consistent, i.e $\bar{\mathbb{D}} \neq \bar{\mathbb{C}}^{-1}$. When we use the new finite Eshelby tensors this situation is significantly improved. For the effective bulk modulus, the new scheme is self consistent, i.e., the two $\bar{\kappa}$ in Eqs. (36) and (38) are equal. The estimated effective shear modulus is not self consistent, but it is quite close as shown in Fig. 2.

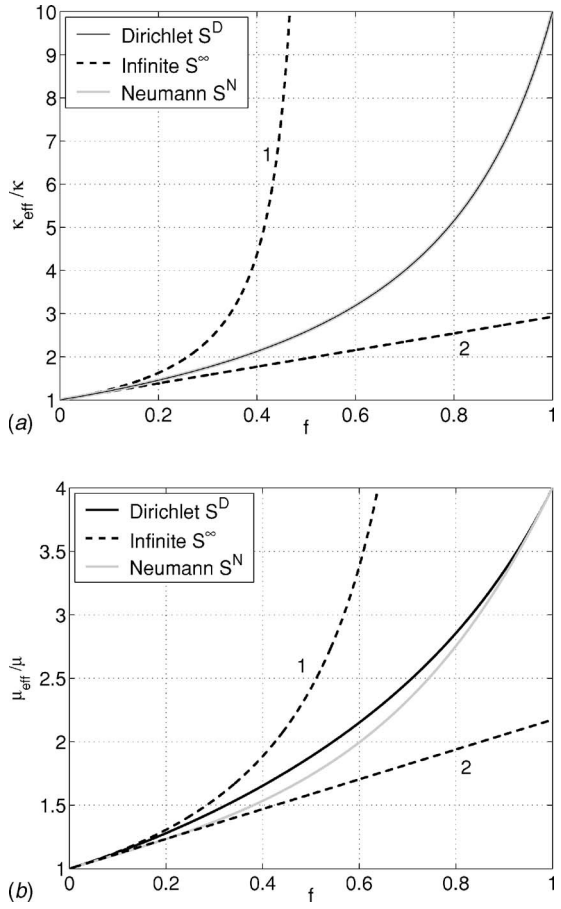

Fig. 2 Effective moduli $\bar{\kappa}$, $\bar{\mu}$ (or κ_{eff} and μ_{eff}) obtained by using the dilute suspension method

3.2 A Refined Mori–Tanaka Model. The original Mori and Tanaka model [11] is derived for an infinite RVE. In the following, we rederive the Mori–Tanaka estimate for a two-phase composite in a finite RVE.

In reality, the boundary condition of an RVE is neither a prescribed displacement boundary condition nor is it a prescribed traction boundary condition. One can thus define a "general finite Eshelby tensor" as the linear combination of the Dirichlet–Eshelby tensor and the Neumann–Eshelby tensor corresponding to general boundary conditions

$$\mathbb{S}^{\cdot,F} = \alpha \mathbb{S}^{\cdot,D} + (1-\alpha)\mathbb{S}^{\cdot,N}, \quad \cdot = I, \text{ or } E \tag{39}$$

For detailed justification, derivation, and discussion of this concept, readers are referred to Ref. [12].

The essence of the Mori–Tanaka procedure is the following incremental homogenization procedure. Let us denote the current background strain of the RVE as $\langle \boldsymbol{\epsilon}^b \rangle_\Omega$, which may or may not be the average strain of the RVE. Adding an inclusion (or a cluster of inclusions represented by a single inclusion) into the RVE, the new average strain $\langle \boldsymbol{\epsilon} \rangle$ in each phase will be the sum of the background strain and the disturbance strain

$$\langle \boldsymbol{\epsilon} \rangle_{\Omega_I} = \langle \boldsymbol{\epsilon}^b \rangle_\Omega + \langle \boldsymbol{\epsilon}^d \rangle_{\Omega_I} \tag{40}$$

$$\langle \boldsymbol{\epsilon} \rangle_{\Omega_E} = \langle \boldsymbol{\epsilon}^b \rangle_\Omega + \langle \boldsymbol{\epsilon}^d \rangle_{\Omega_E} \tag{41}$$

The classical Tanaka–Mori Lemma states that $\langle \boldsymbol{\epsilon}^d \rangle_{\Omega_E} = 0$. This is only true when the RVE is infinite, since $\langle \mathbb{S}^{E,\infty} \rangle_{\Omega_E} = 0$. For a finite RVE, we have to take into account the change of the effective material properties in the matrix

$$\langle \boldsymbol{\epsilon} \rangle_{\Omega_I} = \langle \boldsymbol{\epsilon}^b \rangle_\Omega + \langle \mathbb{S}^{I,F} \rangle_{\Omega_I} : \boldsymbol{\epsilon}^* \tag{42}$$

$$\langle \boldsymbol{\epsilon} \rangle_{\Omega_E} = \langle \boldsymbol{\epsilon}^b \rangle_\Omega + \langle \mathbb{S}^{E,F} \rangle_{\Omega_E} : \boldsymbol{\epsilon}^* \tag{43}$$

Consider the average stress consistency condition (for $\mathbf{x} \in \Omega_I$)

$$\mathbb{C}^I : \langle \boldsymbol{\epsilon} \rangle_{\Omega_I} = \mathbb{C} : (\langle \boldsymbol{\epsilon} \rangle_{\Omega_I} - \boldsymbol{\epsilon}^*) \tag{44}$$

Solving Eqs. (44) for $\langle \boldsymbol{\epsilon} \rangle_{\Omega_I}$ yields

$$\langle \boldsymbol{\epsilon} \rangle_{\Omega_I} = \mathbb{A} : \boldsymbol{\epsilon}^* \tag{45}$$

where $\mathbb{A} = (\mathbb{C} - \mathbb{C}^I)^{-1} : \mathbb{C}$. Considering Eq. (42), we can express the eigenstrain in terms of the background strain as

$$\boldsymbol{\epsilon}^* = [\mathbb{A} - \langle \mathbb{S}^{I,F} \rangle_{\Omega_I}]^{-1} : \langle \boldsymbol{\epsilon}^b \rangle_\Omega \tag{46}$$

Considering the basic average equation of the strain

$$\langle \boldsymbol{\epsilon} \rangle_\Omega = f \langle \boldsymbol{\epsilon} \rangle_{\Omega_I} + (1-f) \langle \boldsymbol{\epsilon} \rangle_{\Omega_E} \tag{47}$$

and substituting Eqs. (42), (43), and (46) into Eq. (47), we can express the average strain $\langle \boldsymbol{\epsilon} \rangle_\Omega$ in terms of the background strain as

$$\langle \boldsymbol{\epsilon} \rangle_\Omega = \mathcal{A}^F : \langle \boldsymbol{\epsilon}^b \rangle_\Omega \tag{48}$$

Here $\mathcal{A}^F$ is the concentration tensor defined as

$$\mathcal{A}^F = [\mathbb{A} - (1-f)(\langle \mathbb{S}^{I,F} \rangle_{\Omega_I} - \langle \mathbb{S}^{E,F} \rangle_{\Omega_E})] : (\mathbb{A} - \langle \mathbb{S}^{I,F} \rangle_{\Omega_I})^{-1} \tag{49}$$

By virtue of Eqs. (45) and (46), the average stress field inside the inclusion can now be written as

$$\langle \boldsymbol{\sigma} \rangle_{\Omega_I} = \mathbb{C} : (\mathbb{A} - \mathbb{I}^{(4s)}) : (\mathbb{A} - \langle \mathbb{S}^{I,F} \rangle_{\Omega_I})^{-1} : \langle \boldsymbol{\epsilon}^b \rangle_\Omega \tag{50}$$

Applying the basic equation for mixture to the stress field,

$$\langle \boldsymbol{\sigma} \rangle_\Omega = f \langle \boldsymbol{\sigma} \rangle_{\Omega_I} + (1-f) \langle \boldsymbol{\sigma} \rangle_{\Omega_E} \tag{51}$$

and substituting Eqs. (42), (43), and (46) into Eq. (51), we can express the average stress $\langle \boldsymbol{\sigma} \rangle_\Omega$ in terms of the background strain as

$$\langle \boldsymbol{\sigma} \rangle_\Omega = \mathcal{B}^F : \langle \boldsymbol{\epsilon}^b \rangle_\Omega \tag{52}$$

with

$$\mathcal{B}^F = \mathbb{C} : [\mathbb{A} - f\mathbb{I}^{(4s)} - (1-f)(\langle \mathbb{S}^{I,F} \rangle_{\Omega_I} - \langle \mathbb{S}^{E,F} \rangle_{\Omega_E})] : (\mathbb{A} - \langle \mathbb{S}^{I,F} \rangle_{\Omega_I})^{-1} \tag{53}$$

Finally from $\langle \boldsymbol{\sigma} \rangle_\Omega = \bar{\mathbb{C}} : \langle \boldsymbol{\epsilon} \rangle_\Omega$, we obtain the effective elastic tensor

$$\bar{\mathbb{C}} = \mathbb{C} - f\mathbb{C} : [\mathbb{A} - (1-f)(\langle \mathbb{S}^{I,F} \rangle_{\Omega_I} - \langle \mathbb{S}^{E,F} \rangle_{\Omega_E})]^{-1}, \quad \bar{\mathbb{D}} = \bar{\mathbb{C}}^{-1} \tag{54}$$

We note in passing that this model is self consistent.

The homogenization procedure with finite Eshelby tensors, $\mathbb{S}^{I,F}$ and $\mathbb{S}^{E,F}$, furnishes a refined Mori–Tanaka model. For isotropic two-phase composites, the corresponding formulas are

$$\bar{\kappa} = \kappa - f\kappa \left[\frac{1}{1 - \kappa^I/\kappa} - (1-f)\Delta s_1^F \right]^{-1},$$

$$\bar{\mu} = \mu - f\mu \left[\frac{1}{1 - \mu^I/\mu} - (1-f)\Delta s_2^F \right]^{-1} \tag{55}$$

Note that the differences $\Delta s_1^F = s_1^{I,F} - s_1^{E,F}$ and $\Delta s_2^F = s_2^{I,F} - s_2^{E,F}$ are given by Eqs. (18)–(20).

Figure 3 displays the profiles of the normalized effective moduli $\bar{\kappa}/\kappa$ and $\bar{\mu}/\mu$ over the volume fraction of the second phase. The same material data is used for the results shown in Fig. 2.

In the case of the bulk modulus the dark, dashed and the light curves match exactly, i.e., they are the same analytically. Indeed, $\bar{\kappa}$ in Eq. (55) is mathematically identical when applying $\mathbb{S}^{\cdot,\infty}$, $\mathbb{S}^{\cdot,D}$,

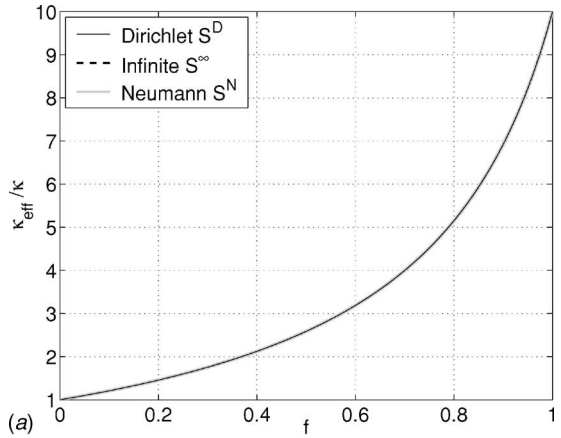

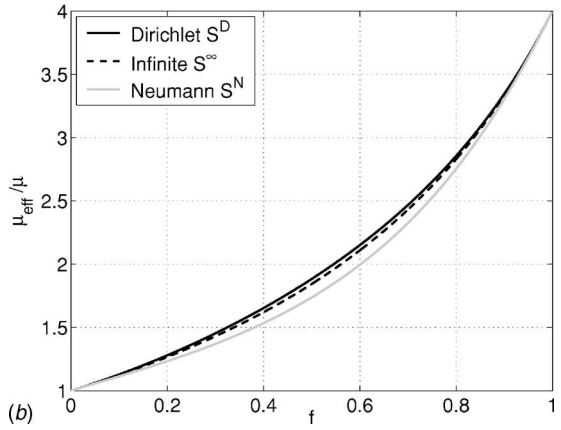

Fig. 3 Effective moduli $\bar{\kappa}$, $\bar{\mu}$ (or κ_{eff} and μ_{eff}) obtained by using the Mori–Tanaka method

or $\mathbb{S}^{\cdot,N}$, since $\Delta s_1^{\infty}=\Delta s_1^{D}=\Delta s_1^{N}$ as noted in Eq. (18). For the shear modulus $\bar{\mu}$ Eq. (55) gives three distinct lines when applying $\mathbb{S}^{\cdot,\infty}$, $\mathbb{S}^{\cdot,D}$, or $\mathbb{S}^{\cdot,N}$.

Remarkably, when comparing Figs. 2 and 3, we find that the dark and light lines match exactly. In other words, it can be shown that by using the finite Eshelby tensors, the dilute suspension method Eqs. (35) and (37) is equivalent to the Mori–Tanaka method Eq. (54), when using the corresponding $\mathbb{S}^{\cdot,D}$ and $\mathbb{S}^{\cdot,N}$. The finite Eshelby tensors $\mathbb{S}^{\cdot,D}$ and $\mathbb{S}^{\cdot,N}$ unify the previously distinct homogenization methods.

4 Exterior/Interior Eigenstrain Method

In the classical eigenstrain homogenization method, since the ambient space (i.e., matrix phase) is assumed to be unbounded, the eigenstrain can only be prescribed inside the inclusion. Therefore the stress or strain consistency condition, i.e., the equivalent eigenstrain principle, is only applicable to the interior. Considering the eigenstrain to be prescribed in the interior domain is the case we have considered so far.

For a finite RVE, the equivalent eigenstrain principle can be equally applied to its interior (inclusion phase) or exterior region (matrix phase). By treating the interior and exterior homogenization scheme with equal footing, one may be able to characterize certain patterns of the phase distribution in an RVE in addition to merely considering the volume fraction of the phases. Such patterns may be the concentration of inhomogeneities towards the center or boundary of the RVE. The exterior eigenstrain method has been studied before by Castles and Mura [13], however, without the knowledge of the finite Eshelby tensor. In this section, we first discuss the exterior eigenstrain method, which relies on the interior eigenstrain results previously obtained. Second we introduce a method which considers the simultaneous prescription of interior and exterior eigenstrains.

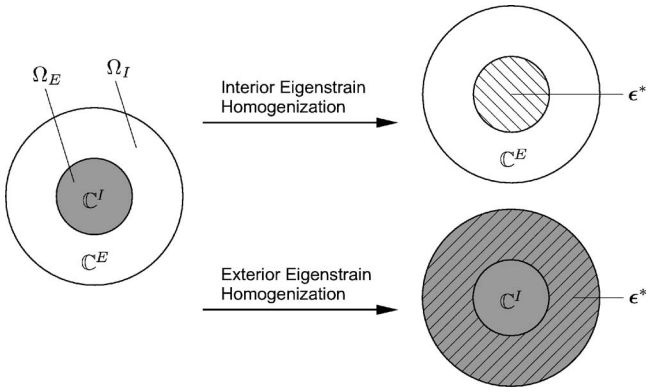

Fig. 4 Illustration of interior and exterior eigenstrain method

4.1 Exterior Eigenstrain Method. Analogously to the interior eigenstrain method, the idea of the exterior eigenstrain method is as follows. We choose the interior phase, characterized by elasticity $\mathbb{C}^I$, as the comparison solid of the RVE. To account for the difference of elastic properties, a uniform eigenstrain is prescribed in the *exterior* region of the RVE, i.e.

$$\boldsymbol{\epsilon}^*(\mathbf{x})=\begin{cases}0, & \forall \mathbf{x}\in\Omega_I\\ \boldsymbol{\epsilon}^*, & \forall \mathbf{x}\in\Omega_E\end{cases} \tag{56}$$

The concept is illustrated in Fig. 4.

It follows that the constitutive relation between the disturbance stress and strain fields has the form

$$\boldsymbol{\sigma}^d(\mathbf{x})=\mathbb{C}^I:[\boldsymbol{\epsilon}^d(\mathbf{x})-\boldsymbol{\epsilon}^*(\mathbf{x})],\quad \forall\,\mathbf{x}\in\Omega \tag{57}$$

Accordingly, Somigliana's identity reads

$$u_m^d(\mathbf{x})=-\int_{\Omega_E}\mathbb{C}^I_{ijk\ell}G^{\infty}_{im,j}(\mathbf{x}-\mathbf{y})d\Omega_y\varepsilon^*_{k\ell}+\int_{\partial\Omega}\mathbb{C}^I_{ijk\ell}u^d_k(\mathbf{y})G^{\infty}_{im,j}(\mathbf{x}-\mathbf{y})n_\ell(\mathbf{y})dS_y+\int_{\partial\Omega}\mathbb{C}^I_{ijk\ell}u^d_{k,\ell}(\mathbf{y})n_j(\mathbf{y})G^{\infty}_{im}(\mathbf{x}-\mathbf{y})dS_y \tag{58}$$

By considering either the Dirichlet or Neumann boundary condition prescribed on the RVE boundary, the above equation can be solved to relate the disturbance strain field to the prescribed *exterior* eigenstrain through the so called *exterior Eshelby tensors* denoted by $\bar{\mathbb{S}}^{\cdot,\star}$. They are defined from

$$\boldsymbol{\epsilon}^d(\mathbf{x})=\begin{cases}\bar{\mathbb{S}}^{E,\star}(\mathbf{x}):\boldsymbol{\epsilon}^*, & \forall\,\mathbf{x}\in\Omega_E\\ \bar{\mathbb{S}}^{I,\star}(\mathbf{x}):\boldsymbol{\epsilon}^*, & \forall\,\mathbf{x}\in\Omega_I\end{cases} \tag{59}$$

where the superscripts $\cdot=I$ or E denote the tensors evaluated at the interior or exterior regions, and where $\star=D$ or N stands for either the Dirichlet (prescribed displacement) or Neumann boundary (prescribed traction) condition.

The disturbance fields in Eq. (58) can be solved exactly by means of superposition. Since $\Omega_E=\Omega/\Omega_I$ the resulting exterior eigenstrain Eshelby tensors can be written as a combination of the interior eigenstrain Eshelby tensors, which have been solved in Part I, as

$$\bar{\mathbb{S}}^{E,\star}=\mathbb{S}^{I,\star}(\mathbb{C}^I,f=1)-\mathbb{S}^{E,\star}(\mathbb{C}^I,f_I),\quad \mathbf{x}\in\Omega_E \tag{60}$$

$$\bar{\mathbb{S}}^{I,\star}=\mathbb{S}^{I,\star}(\mathbb{C}^I,f=1)-\mathbb{S}^{I,\star}(\mathbb{C}^I,f_I),\quad \mathbf{x}\in\Omega_I \tag{61}$$

We emphasize that for this case (the exterior eigenstrain method) the Eshelby tensor $\mathbb{S}^{\cdot,\star}$ in the above equations takes the material

property $\mathbb{C}^I$ of the inclusion (the comparison solid), and the volume fraction f_I of the inclusion phase. Given the boundary condition $\star=D$ or N, the first term of the equations above can be easily evaluated (see Part I for the expressions of $\mathbb{S}^{I,\star}$)

$$\mathbb{S}^{I,D}(\mathbb{C}^I, f=1)=\mathbb{O}$$

and

$$\mathbb{S}^{I,N}(\mathbb{C}^I, f=1)=\mathbb{I}^s \tag{62}$$

where $\mathbb{O}$ and $\mathbb{I}^s$ are the fourth-order zero tensor and identity tensor, respectively. Therefore the exterior eigenstrain Eshelby tensors can be related explicitly to the interior eigenstrain Eshelby tensors by

$$\bar{\mathbb{S}}^{\star,D}=-\mathbb{S}^{\star,D}(\mathbb{C}^I,f_I), \quad \mathbf{x}\in\Omega \tag{63}$$

$$\bar{\mathbb{S}}^{\star,N}=\mathbb{I}^s-\mathbb{S}^{\star,N}(\mathbb{C}^I,f_I), \quad \mathbf{x}\in\Omega \tag{64}$$

To proceed further, the average of the exterior eigenstrain Eshelby tensors $\bar{\mathbb{S}}^{\star,\star}$ is needed. Following Sec. 2, we find

$$\langle \bar{S}^{I,\star}_{ijmn}\rangle_{\Omega_I}=\bar{s}_1^{I,\star}\mathbb{E}^{(1)}_{ijmn}+\bar{s}_2^{I,\star}\mathbb{E}^{(2)}_{ijmn} \tag{65}$$

$$\langle \bar{S}^{E,\star}_{ijmn}\rangle_{\Omega_E}=\bar{s}_1^{E,\star}\mathbb{E}^{(1)}_{ijmn}+\bar{s}_2^{E,\star}\mathbb{E}^{(2)}_{ijmn} \tag{66}$$

with

$$\bar{s}_1^{I,D}=-\frac{(1+\nu)(1-f)}{3(1-\nu)}, \quad \bar{s}_2^{I,D}=-\frac{2(4-5\nu)(1-f)}{15(1-\nu)}+21\gamma_u(1-f^{2/3})$$

$$\bar{s}_1^{E,D}=\frac{(1+\nu)f}{3(1-\nu)}, \quad \bar{s}_2^{E,D}=\frac{2(4-5\nu)f}{15(1-\nu)}-21\gamma_u f\frac{1-f^{2/3}}{1-f} \tag{67}$$

for the Dirichlet BVP and

$$\bar{s}_1^{I,N}=\frac{2(1-2\nu)(1-f)}{3(1-\nu)}, \quad \bar{s}_2^{I,N}=\frac{(7-5\nu)(1-f)}{15(1-\nu)}-21\gamma_t(1-f^{2/3})$$

$$\bar{s}_1^{E,N}=1-\frac{2(1-2\nu)f}{3(1-\nu)}, \quad \bar{s}_2^{E,N}=1-\frac{(7-5\nu)f}{15(1-\nu)}+21\gamma_t f\frac{1-f^{2/3}}{1-f} \tag{68}$$

for the Neumann BVP. Here γ_u and γ_t are as given in Eq. (14). Note that we have omitted all superscripts on the right hand sides, with the understanding that all material properties in the above expressions (and in γ_u and γ_t) are in terms of the inclusion phase (i.e., $\nu=\nu_I$). Further, the volume fraction above is that of the inclusion (i.e., $f=f_I$). Substituting $f_I=1-f_E$ above and comparing Eqs. (67) and (68) with Eqs. (10)–(13), the following connections can be established between the exterior and interior eigenstrain Eshelby tensors

$$\bar{s}_1^{I,\star}(\nu,f_E)=s_1^{E,\star}(\nu,f_I), \quad \bar{s}_2^{I,\star}(\nu,f_E)\approx s_2^{E,\star}(\nu,f_I) \tag{69}$$

$$\bar{s}_1^{E,\star}(\nu,f_E)=s_1^{I,\star}(\nu,f_I), \quad \bar{s}_2^{E,\star}(\nu,f_E)\approx s_2^{I,\star}(\nu,f_I) \tag{70}$$

where $\star=D,N$. Note that the equality holds between the bulk coefficients s_1, whereas the deviatoric coefficients s_2 are only approximately equal. Likewise we can substitute $f_I=1-f_E$ into Eqs. (10)–(13) and compare these equations to Eqs. (67) and (68). Then we obtain

$$\bar{s}_1^{I,\star}(\nu,f_I)=s_1^{E,\star}(\nu,f_E), \quad \bar{s}_2^{I,\star}(\nu,f_I)\approx s_2^{E,\star}(\nu,f_E) \tag{71}$$

$$\bar{s}_1^{E,\star}(\nu,f_I)=s_1^{I,\star}(\nu,f_E), \quad \bar{s}_2^{E,\star}(\nu,f_I)\approx s_2^{I,\star}(\nu,f_E) \tag{72}$$

Next we consider the Mori–Tanaka model as an example to illustrate the exterior eigenstrain method and its relation to the interior eigenstrain method. Recall the Mori–Tanaka formula for the interior eigenstrain homogenization Eq. (54)

$$\bar{\mathbb{C}}=\mathbb{C}^E-f_I\mathbb{C}^E:\{(\mathbb{C}^E-\mathbb{C}^I)^{-1}:\mathbb{C}^E-f_E[\langle \mathbb{S}^{I,\star}(\mathbb{C}^E,f_I)\rangle_{\Omega_I}-\langle \mathbb{S}^{E,\star}(\mathbb{C}^E,f_I)\rangle_{\Omega_E}]\}^{-1} \tag{73}$$

Let us consider a two-phase composite with elasticities $\mathbb{C}_1$ and $\mathbb{C}_2$. Geometrically, the two phases can be arranged in two ways. We either let phase 1 be the matrix and phase 2 the inclusion ($\mathbb{C}^E=\mathbb{C}_1$, $\mathbb{C}^I=\mathbb{C}_2$) or vice versa ($\mathbb{C}^I=\mathbb{C}_1$, $\mathbb{C}^E=\mathbb{C}_2$). The equation above then takes the two forms

$$\bar{\mathbb{C}}=\mathbb{C}_1-f_2\mathbb{C}_1:\{(\mathbb{C}_1-\mathbb{C}_2)^{-1}:\mathbb{C}_1-f_1[\langle \mathbb{S}^{I,\star}(\mathbb{C}_1,f_2)\rangle_{\Omega_I}-\langle \mathbb{S}^{E,\star}(\mathbb{C}_1,f_2)\rangle_{\Omega_E}]\}^{-1} \tag{74}$$

$$\bar{\mathbb{C}}=\mathbb{C}_2-f_1\mathbb{C}_2:\{(\mathbb{C}_2-\mathbb{C}_1)^{-1}:\mathbb{C}_2-f_2[\langle \mathbb{S}^{I,\star}(\mathbb{C}_2,f_1)\rangle_{\Omega_I}-\langle \mathbb{S}^{E,\star}(\mathbb{C}_2,f_1)\rangle_{\Omega_E}]\}^{-1} \tag{75}$$

Reexamining the Mori–Tanaka method via exterior eigenstrain homogenization, we obtain

$$\bar{\mathbb{C}}=\mathbb{C}^I-f_E\mathbb{C}^I:\{(\mathbb{C}^I-\mathbb{C}^E)^{-1}:\mathbb{C}^I-f_I[\langle \bar{\mathbb{S}}^{E,\star}(\mathbb{C}^I,f_I)\rangle_{\Omega_E}-\langle \bar{\mathbb{S}}^{I,\star}(\mathbb{C}^I,f_I)\rangle_{\Omega_I}]\}^{-1} \tag{76}$$

which we call *the exterior eigenstrain Mori–Tanaka formula*. For a two-phase composite with elastic stiffnesses $\mathbb{C}_1$ and $\mathbb{C}_2$, we then have

$$\bar{\mathbb{C}}=\mathbb{C}_2-f_1\mathbb{C}_2:\{(\mathbb{C}_2-\mathbb{C}_1)^{-1}:\mathbb{C}_2-f_2[\langle \bar{\mathbb{S}}^{E,\star}(\mathbb{C}_2,f_2)\rangle_{\Omega_E}-\langle \bar{\mathbb{S}}^{I,\star}(\mathbb{C}_2,f_2)\rangle_{\Omega_I}]\}^{-1} \tag{77}$$

$$\bar{\mathbb{C}}=\mathbb{C}_1-f_2\mathbb{C}_1:\{(\mathbb{C}_1-\mathbb{C}_2)^{-1}:\mathbb{C}_1-f_1[\langle \bar{\mathbb{S}}^{E,\star}(\mathbb{C}_1,f_1)\rangle_{\Omega_E}-\langle \bar{\mathbb{S}}^{I,\star}(\mathbb{C}_1,f_1)\rangle_{\Omega_I}]\}^{-1} \tag{78}$$

Equations (74), (75), (77), and (78) constitute the four flavors of the Mori–Tanaka method. In view of relations (69)–(72) we can see that Eq. (77) is approximately equal to Eq. (75) and that Eq. (78) is approximately equal to Eq. (74). In fact, for the effective bulk modulus $\bar{\kappa}$ this approximation becomes an equality. For the effective shear modulus $\bar{\mu}$, however, there are slight differences. These differences can be seen in Fig. 5, which shows the effective shear modulus $\bar{\mu}$ for the four cases.

The material properties used in the calculation are $\kappa_2=4\kappa_1$, $\mu_2=10\mu_1$, and $\nu_2=0.3$. The traction boundary condition ($\star=N$) is used in the calculation. One can see how close the pairs 1, 4 and 2, 3 are. In the case of the effective bulk modulus these pairs are equal. We can therefore conclude that exchanging the material phases is approximately equal to exchanging the regions where the eigenstrain is prescribed.

This, however, does not mean that the exterior eigenstrain method has no technical merits. In the following sections we shall discuss two new models that are built upon the idea of the exterior eigenstrain method. The first, the dual eigenstrain method, furnishes a method that allows the smooth transition between curves 1 and 3 or between 2 and 4. Second, in Sec. 5, the shell model, a novel multiphase model, is a further generalization of this idea.

4.2 Dual Eigenstrain Method. We have seen in Fig. 5 that, for fixed phase distribution, the interior and exterior eigenstrain methods give very different homogenization results (i.e., the difference between 1 and 3 or between 2 and 4). We therefore want to consider a model that prescribes an eigenstrain field in both the interior and exterior regions of the inclusion simultaneously

$$\boldsymbol{\epsilon}^*(\mathbf{x})=\begin{cases}\boldsymbol{\epsilon}_I^*, & \forall \mathbf{x}\in\Omega_I\\ \boldsymbol{\epsilon}_E^*, & \forall \mathbf{x}\in\Omega_E\end{cases} \tag{79}$$

The model, termed the *dual eigenstrain method* is discussed in

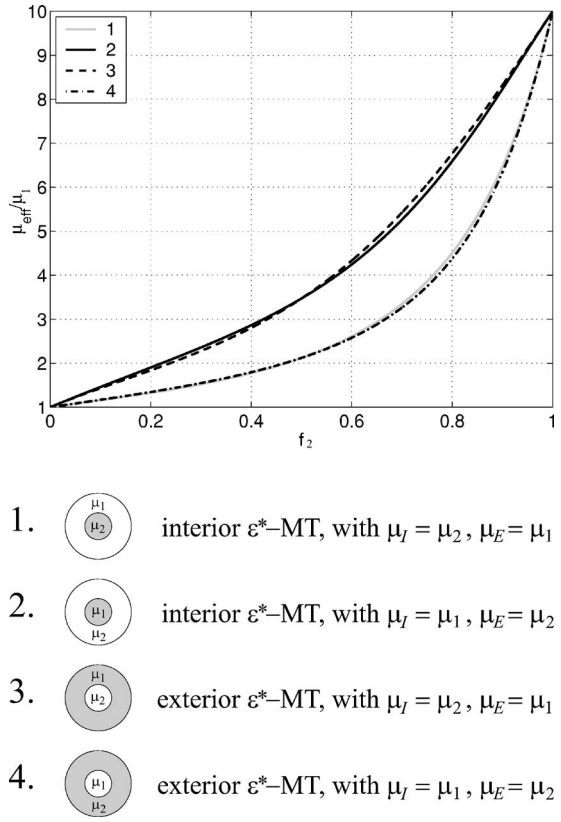

Fig. 5 Mori–Tanaka homogenization for the interior and exterior eigenstrain methods

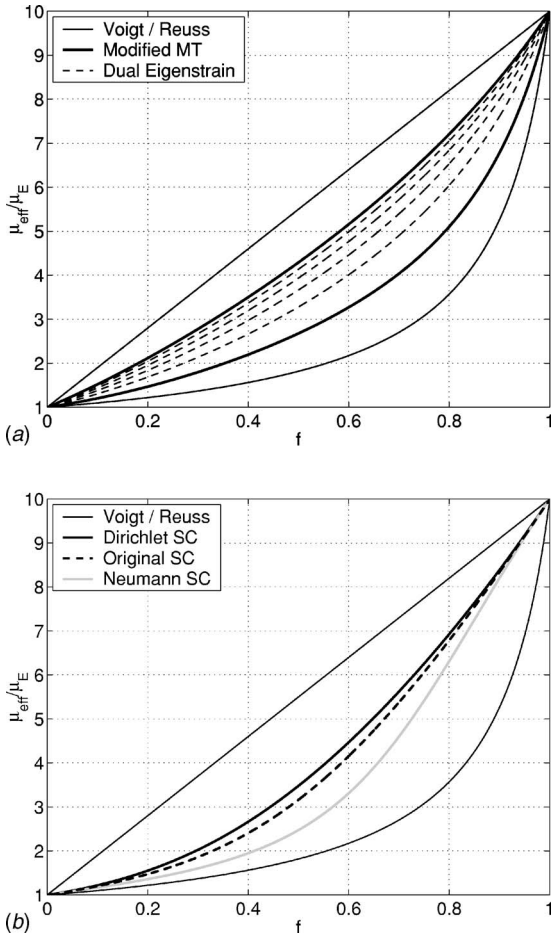

Fig. 6 Effective shear modulus for: (*a*) $\widetilde{\mathbb{C}} = a\mathbb{C}^I + (1-a)\mathbb{C}^E$, and (*b*) $\widetilde{\mathbb{C}} = \overline{\mathbb{C}}$

detail in Ref. [12] and we only illustrate the main concept of the method here. The central idea of the *dual eigenstrain method* is to treat the homogenization of both the inclusion and matrix phase equally. Such a model has no preference between the two material phases, because neither phase is chosen as the reference state. The comparison solid for the RVE is rather characterized by $\widetilde{\mathbb{C}}$, which can be considered as an estimate of the effective modulus $\overline{\mathbb{C}}$. Concrete choices for $\widetilde{\mathbb{C}}$ are considered later.

Denoting the average background strain as $\boldsymbol{\epsilon}^b$, the dual stress consistency conditions then become

$$\mathbb{C}^I:[\boldsymbol{\epsilon}^b + \boldsymbol{\epsilon}^d(\mathbf{x})] = \widetilde{\mathbb{C}}:[\boldsymbol{\epsilon}^b + \boldsymbol{\epsilon}^d(\mathbf{x}) - \boldsymbol{\epsilon}_I^*), \quad \forall\, \mathbf{x} \in \Omega_I \tag{80}$$

$$\mathbb{C}^E:[\boldsymbol{\epsilon}^b + \boldsymbol{\epsilon}^d(\mathbf{x})) = \widetilde{\mathbb{C}}:(\boldsymbol{\epsilon}^b + \boldsymbol{\epsilon}^d(\mathbf{x}) - \boldsymbol{\epsilon}_E^*), \quad \forall\, \mathbf{x} \in \Omega_E \tag{81}$$

The disturbance strain field $\boldsymbol{\epsilon}^d$ is the superposition of the disturbance strain field due to the interior eigenstrain and the disturbance strain field due to the exterior eigenstrain field, i.e.

$$\boldsymbol{\epsilon}^d(\mathbf{x}) = \begin{cases} \mathbb{S}^{I,\star}:\boldsymbol{\epsilon}_I^* + \overline{\mathbb{S}}^{I,\star}:\boldsymbol{\epsilon}_E^*, & \forall \mathbf{x} \in \Omega_I \\ \mathbb{S}^{E,\star}:\boldsymbol{\epsilon}_I^* + \overline{\mathbb{S}}^{E,\star}:\boldsymbol{\epsilon}_E^*, & \forall \mathbf{x} \in \Omega_E \end{cases} \tag{82}$$

Here $\mathbb{S}^{\cdot,\star}$ is the interior eigenstrain finite Eshelby tensor as derived in Part I and $\overline{\mathbb{S}}^{\cdot,\star}$ is the exterior eigenstrain Eshelby tensor as given in the preceding section; (both accepting $\cdot = I$ or E and $\star = D$ or N). Both $\mathbb{S}^{\cdot,\star}$ and $\overline{\mathbb{S}}^{\cdot,\star}$ take $\widetilde{\mathbb{C}}$ as the comparison solid. We note that the dual eigenstrain method contains the two special cases $\boldsymbol{\epsilon}_E^* = 0$, with $\widetilde{\mathbb{C}} = \mathbb{C}^E$ and $\boldsymbol{\epsilon}_I^* = 0$, with $\widetilde{\mathbb{C}} = \mathbb{C}^I$, which are the interior and exterior eigenstrain methods, respectively.

From here on the derivation proceeds in a similar manner as the interior eigenstrain case (see Sec. 3). The effective elasticity modulus is obtained as

$$\overline{\mathbb{C}} = [f\mathbb{C}^I:\mathcal{A}_E + (1-f)\mathbb{C}^E:\mathcal{A}_I]:[f\mathcal{A}_E + (1-f)\mathcal{A}_I]^{-1} \tag{83}$$

with the concentration tensors

$$\mathcal{A}_E = \mathbb{I}^s - \widetilde{\mathbb{C}}^{-1}:(\widetilde{\mathbb{C}} - \mathbb{C}^E):\Delta\mathbb{S}^\star$$

$$\mathcal{A}_I = \mathbb{I}^s - \widetilde{\mathbb{C}}^{-1}:(\widetilde{\mathbb{C}} - \mathbb{C}^I):\Delta\mathbb{S}^\star \tag{84}$$

and the difference

$$\Delta\mathbb{S}^\star := \langle \mathbb{S}^{I,\star}(\widetilde{\mathbb{C}}, f = f_I)\rangle_{\Omega_E} - \langle \mathbb{S}^{E,\star}(\widetilde{\mathbb{C}}, f = f_I)\rangle_{\Omega_I} \tag{85}$$

Here we have indicated that $\mathbb{S}^{\cdot,\star}$ depends on the comparison solid $\widetilde{\mathbb{C}}$ and the volume fraction $f = f_I$. We note that the coefficients of $\Delta\mathbb{S}^\star$ follow from Eqs. (18)–(20) given in Sec. 2, with setting $\nu = \widetilde{\nu}$ and $f = f_I$. Choosing either $\widetilde{\mathbb{C}} = \mathbb{C}^E$ or $\widetilde{\mathbb{C}} = \mathbb{C}^I$, the method degenerates to the interior homogenization Eq. (73) or the exterior homogenization Eq. (76), respectively. If we let $\widetilde{\mathbb{C}}$ assume a value between $\mathbb{C}^I$ and $\mathbb{C}^E$, the effective modulus $\overline{\mathbb{C}}$ given by the dual eigenstrain method can be expected to lie in between these two special cases. As an example consider the convex combination

$$\widetilde{\mathbb{C}} = a\mathbb{C}^I + (1-a)\mathbb{C}^E, \quad 0 \leqslant a \leqslant 1 \tag{86}$$

Figure 6(*a*) shows the effective shear modulus $\bar{\mu}$ obtained from Eq. (83) using Eq. (86) for $a = \{0, 0.2, 0.4, 0.6, 0.8, 1\}$.

The material properties have been chosen as before ($\kappa_I = 4\kappa_E$, $\mu_I = 10\mu_E$, and $\nu_E = 0.3$). The boundary condition in Fig. 6(*a*) is chosen as the Dirichlet BC ($\star = D$). We observe that $\bar{\mu}$, computed

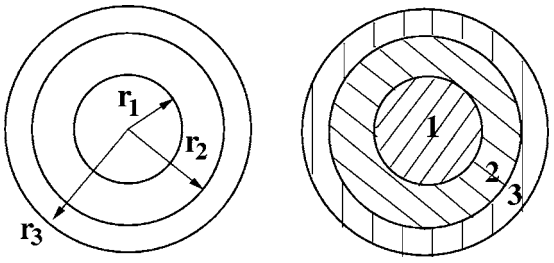

Fig. 7 A three-layer shell model

by the dual eigenstrain method, lies in between the two special cases, the interior and exterior eigenstrain MT method obtained for $a=0$ and $a=1$, respectively. We remark that there are other interesting choices for $\widetilde{\mathbb{C}}$ to consider (see Ref. [12]). For instance, we can use $\widetilde{\mathbb{C}}$ as a predictor of the effective modulus $\overline{\mathbb{C}}$. One such predictor is the Voigt bound. Equation (83) then becomes a corrected value for $\overline{\mathbb{C}}$. This predictor–corrector scheme can be viewed as a generalization of the classical self-consistent method. An implicit self-consistent method arises when considering $\widetilde{\mathbb{C}}=\overline{\mathbb{C}}$ in Eq. (83). The effective shear modulus for this case is shown in Fig. 6(*b*) for both $\star=D$ and N. For comparison the original self-consistent method is also shown. The material data are the same as before.

As a final remark, let us consider the dual eigenstrain method in view of the two possible ways of arranging the material phases. As we have discussed in the preceding section we can either have $\mathbb{C}^E=\mathbb{C}^1$ and $\mathbb{C}^I=\mathbb{C}^2$ or the flipped case $\mathbb{C}^I=\mathbb{C}^1$ and $\mathbb{C}^E=\mathbb{C}^2$. Thus the dual eigenstrain method Eq. (83) results in two distinct formulas.

5 A Shell Model

To utilize the finite Eshelby tensors to represent different microstructures, a so-called spherical shell model is developed, that is a n-phase composite RVE modeled by n concentric spherical shells. To illustrate the model, we present the detailed study of a three-layer shell model (see Fig. 7).

For the three-layer shell model, the RVE consists of three concentric spherical shells, which are labeled as

$$\Omega_1(\mathbf{x})=\{\mathbf{x}||\mathbf{x}|<r_1\},\quad \Omega_2(\mathbf{x})=\{\mathbf{x}|r_1<|\mathbf{x}|<r_2\},$$

$$\Omega_3(\mathbf{x})=\{\mathbf{x}|r_2<|\mathbf{x}|<r_3\}$$

Here the radius of the RVE is r_3, and the volume fraction of the three shells are

$$f_1=\left(\frac{r_1}{r_3}\right)^3,\quad f_2=\frac{r_2^3-r_1^3}{r_3^3},\quad f_3=\frac{r_3^3-r_2^3}{r_3^3} \tag{87}$$

with

$$f_1+f_2+f_3=1$$

To derive the Eshelby tensors for each shell, we consider three partially overlapped concentric spheres

$$\Omega_{\mathrm{I}}(\mathbf{x})=\{\mathbf{x}||\mathbf{x}|<r_1\},\quad \Omega_{\mathrm{II}}(\mathbf{x})=\{\mathbf{x}||\mathbf{x}|<r_2\},\quad \Omega_{\mathrm{III}}(\mathbf{x})=\{\mathbf{x}||\mathbf{x}|<r_3\}$$

The interior and exterior Eshelby tensors for each sphere Ω_J are denoted as

$$\mathbb{S}^{J,F}(\mathbf{x}):=\begin{cases}\mathbb{S}^{I,F}(\mathbf{x}), & \forall\mathbf{x}\in\Omega_J,\quad J=\mathrm{I,II,III}\\ \mathbb{S}^{E,F}(\mathbf{x}), & \forall\mathbf{x}\in\Omega/\Omega_J,\quad J=\mathrm{I,II,III}\end{cases} \tag{88}$$

where the superscript F represents the general boundary conditions, see Eq. (39). Subsequently the average of the Eshelby tensor is required for each shell. We first denote the average of the Eshelby tensor of the overlapping spheres

$$\mathbb{S}^{Jj,F}:=\langle\mathbb{S}^{J,F}\rangle_{\Omega_j},\quad J=\mathrm{I,II,III}\quad\text{and } j=1,2,3 \tag{89}$$

where the first superscript J (Roman numbers) denotes the sphere, Ω_J, in which the eigenstrain is prescribed, and where the second superscript j (Arabic numbers) denotes the shell, Ω_j, over which the average is taken. Similarly we denote the average Eshelby tensor of the shell domains as

$$\mathbb{S}^{ij,F}:=\langle\mathbb{S}^{i,F}\rangle_{\Omega_j},\quad i=1,2,3\quad\text{and } j=1,2,3 \tag{90}$$

Again, the first subscript index, i, refers to the shell region, Ω_i, in which the eigenstrains are prescribed, and the second index, j, denotes the shell region, Ω_j, over which the average is taken. As we have shown in Sec. 2 the average Eshelby tensors can be written as

$$\mathbb{S}^{ij,F}=s_1^{ij,F}\mathbb{E}^{(1)}+s^{ij,F}\mathbb{E}^{(2)},\quad i,j=1,2,3 \tag{91}$$

The idea is to use the Eshelby tensors of three overlapping spheres to represent the Eshelby tensors of the shells via superposition. For the first spherical shell (the inner most shell) we write

$$\mathbb{S}^{11,F}=\mathbb{S}^{I1,F}=s_1^{11,F}\mathbb{E}^{(1)}+s_2^{11,F}\mathbb{E}^{(2)}$$

$$\mathbb{S}^{1j,F}=\mathbb{S}^{Ij,F}=s_1^{1j,F}\mathbb{E}^{(1)}+s_2^{1j,F}\mathbb{E}^{(2)} \tag{92}$$

Here, $s_\alpha^{11,F}$ are the coefficients of the interior Eshelby tensor, whereas $s_\alpha^{1j,F}$, $j=2,3$ are the coefficients of the exterior Eshelby tensors. Using superposition, the Eshelby tensors for the second and third spherical shells can be obtained by using the combination of the average Eshelby tensors of the three overlapping spheres

$$\mathbb{S}^{2i,F}=\mathbb{S}^{\mathrm{II}i,F}-\mathbb{S}^{\mathrm{I}i,F},\quad i=1,2,3 \tag{93}$$

$$\mathbb{S}^{3i,F}=\mathbb{S}^{\mathrm{III}i,F}-\mathbb{S}^{\mathrm{II}i,F},\quad i=1,2,3 \tag{94}$$

Therefore, for $\alpha=1,2$

$$s_\alpha^{2i,F}=s_\alpha^{\mathrm{II}i,F}-s_\alpha^{\mathrm{I}i,F}$$

and

$$s_\alpha^{3i,F}=s_\alpha^{\mathrm{III}i,F}-s_\alpha^{\mathrm{II}i,F},\quad i=1,2,3 \tag{95}$$

To this end, all the coefficients of the Eshelby tensors for each shell layer are expressed in terms the of the Eshelby coefficients for solid spheres, Ω_I, Ω_{II}, and Ω_{III}, which are documented in the Appendix for a three-sphere RVE.

To illustrate the application of the shell model, we consider a simple homogenization example of a two-phase composite material, with elastic modulus $\mathbb{C}_2=\mathbb{C}_e$ in Ω_2 and $\mathbb{C}_1=\mathbb{C}_3=\mathbb{C}$ in Ω_1 and Ω_3. We prescribe the eigenstrain in Ω_2,

$$\boldsymbol{\epsilon}^*(\mathbf{x})=\begin{cases}\boldsymbol{\epsilon}^*, & \forall\mathbf{x}\in\Omega_2\\ 0, & \text{otherwise}\end{cases} \tag{96}$$

We assume the RVE is subjected to the macrostrain boundary condition, i.e., $\mathbf{u}=\boldsymbol{\epsilon}^0\mathbf{x}$, $\forall\mathbf{x}\in\partial\Omega$ and impose the following stress consistency condition

$$\mathbb{C}_e:(\boldsymbol{\epsilon}^0+\boldsymbol{\epsilon}^d)=\mathbb{C}:(\boldsymbol{\epsilon}^0+\boldsymbol{\epsilon}^d-\boldsymbol{\epsilon}^*),\quad \forall\,\mathbf{x}\in\Omega_2 \tag{97}$$

One can then derive the effective elastic stiffness similar to the formula of dilute suspension homogenization Eq. (35)

$$\overline{\mathbb{C}}=\mathbb{C}-f\mathbb{C}:(\mathbb{A}_e-\mathbb{S}^{22,D})^{-1}, \tag{98}$$

where $\mathbb{A}_e=(\mathbb{C}-\mathbb{C}_e)^{-1}:\mathbb{C}$. We note that here $\mathbb{S}^{22,D}$ is a function of both volume fraction of the second phase Ω_2 (i.e., $f=f_2$), and the geometric allocation or separation of the first phase, which can be characterized by a nondimensional parameter $\beta:=f_1/(f_1+f_3)=f_1/(1-f)$. The coefficients of $\mathbb{S}^{22,D}$ are found to be

$$s_1^{22,D}=\frac{(1+\nu)(1-f)}{3(1-\nu)} \tag{99}$$

$$s_2^{22,D} = \frac{8-10\nu}{15(1-\nu)}(1-\beta)(1-f) - 21\gamma_u[\beta(1-f)+f]\cdot\left\{1 - \frac{[\beta(1-f)+f)^{5/3} - [\beta(1-f)]^{5/3}}{f}\right\} + \frac{2\beta(1-f)}{15(1-\nu)} + 21\gamma_u[\beta(1-f)]\frac{f-\beta(1-f)-[\beta(1-f)+f]^{5/3}+[\beta(1-f)]^{5/3}}{f-\beta(1-f)} \quad (100)$$

For the general boundary condition of Eq. (39), the following stress consistency is imposed

$$\mathbb{C}_e:(\boldsymbol{\epsilon}^b+\boldsymbol{\epsilon}^d) = \mathbb{C}:(\boldsymbol{\epsilon}^b+\boldsymbol{\epsilon}^d-\boldsymbol{\epsilon}^*), \quad \forall\, \mathbf{x}\in\Omega_2 \quad (101)$$

This leads to the usual relationships between the average strain and eigenstrain, as well as between the eigenstrain and the background strain, i.e.

$$\langle\boldsymbol{\epsilon}\rangle_{\Omega_2} = \mathbb{A}_e:\boldsymbol{\epsilon}^* \quad (102)$$

and

$$\boldsymbol{\epsilon}^* = (\mathbb{A}_e - \mathbb{S}^{22,F}):\boldsymbol{\epsilon}^b, \quad \text{with } \mathbb{A}_e = (\mathbb{C}-\mathbb{C}_e)^{-1}:\mathbb{C}$$

Then the average strain in the RVE will be

$$\begin{aligned}\langle\boldsymbol{\epsilon}\rangle_\Omega &= f_1\langle\boldsymbol{\epsilon}\rangle_{\Omega_1} + f_2\langle\boldsymbol{\epsilon}\rangle_{\Omega_2} + f_3\langle\boldsymbol{\epsilon}\rangle_{\Omega_3} \\ &= \boldsymbol{\epsilon}^b + f_1\mathbb{S}^{21,F}:\boldsymbol{\epsilon}^* + f_2\mathbb{S}^{22,F}:\boldsymbol{\epsilon}^* + f_3\mathbb{S}^{23,F}:\boldsymbol{\epsilon}^* \\ &= [\mathbb{A}_e + f_1\mathbb{S}^{21,F} - (f_1+f_3)\mathbb{S}^{22,F} + f_3\mathbb{S}^{23,F}]:[\mathbb{A}_e - \mathbb{S}^{22,F}]^{-1}:\boldsymbol{\epsilon}^b\end{aligned} \quad (103)$$

Further, the average stress in the RVE becomes

$$\langle\boldsymbol{\sigma}\rangle_\Omega = f_1\langle\boldsymbol{\sigma}\rangle_{\Omega_1} + f_2\langle\boldsymbol{\sigma}\rangle_{\Omega_2} + f_3\langle\boldsymbol{\sigma}\rangle_{\Omega_3} = \{(f_1\mathbb{C} + f_2\mathbb{C}_e + f_3\mathbb{C}):(\mathbb{A}_e - \mathbb{S}^{22,F}) + [\mathbb{C}(f_1\mathbb{S}^{21,F} + f_3\mathbb{S}^{23,F}) + f_2\mathbb{C}_e\mathbb{S}^{22,F}]\}:(\mathbb{A}_e - \mathbb{S}^{22,F})^{-1}:\boldsymbol{\epsilon}^b \quad (104)$$

Substituting Eq. (103) into Eq. (104) leads to the effective elastic tensor

$$\bar{\mathbb{C}} = \mathbb{C} - f\mathbb{C}:\{\mathbb{A}_e - (1-f)[\mathbb{S}^{22,F} - \beta\mathbb{S}^{21,F} - (1-\beta)\mathbb{S}^{23,F}]\}^{-1}, \quad (105)$$

where $f=f_2$ and

$$\beta = \frac{f_1}{f_1+f_3} = \frac{f_1}{1-f}$$

It is interesting to point out that the above formalism resembles the classical Mori–Tanaka model Eq. (54). For the shell model with the eigenstrain prescribed in Ω_2, the contribution from the exterior Eshelby tensor is represented by a linear combination of $\mathbb{S}^{21,F}$ and $\mathbb{S}^{23,F}$ through parameter $\beta\in[0,1]$, which can be used to characterize the evolution of the microstructure. Figure 8 shows that the microstructure evolution can have some influence on the effective shear modulus. In Fig. 8(*a*), the range of the effective shear modulus for $\beta=0,0.1,\ldots,0.9,1.0$ is plotted for the Dirichlet, Neumann, and averaged ($\alpha=0.5$ in Eq. (39)) boundary conditions, respectively. The differences can be seen more clearly if, for a given volume fraction, the effective modulus is plotted over β. This is shown in Fig. 8(*b*) for the volume fraction $f=0.5$, which demonstrates the dependency of the shell model on the microstructure. Note that this dependency has little influence for the average case but is considerably stronger for both the Dirichlet and Neumann case.

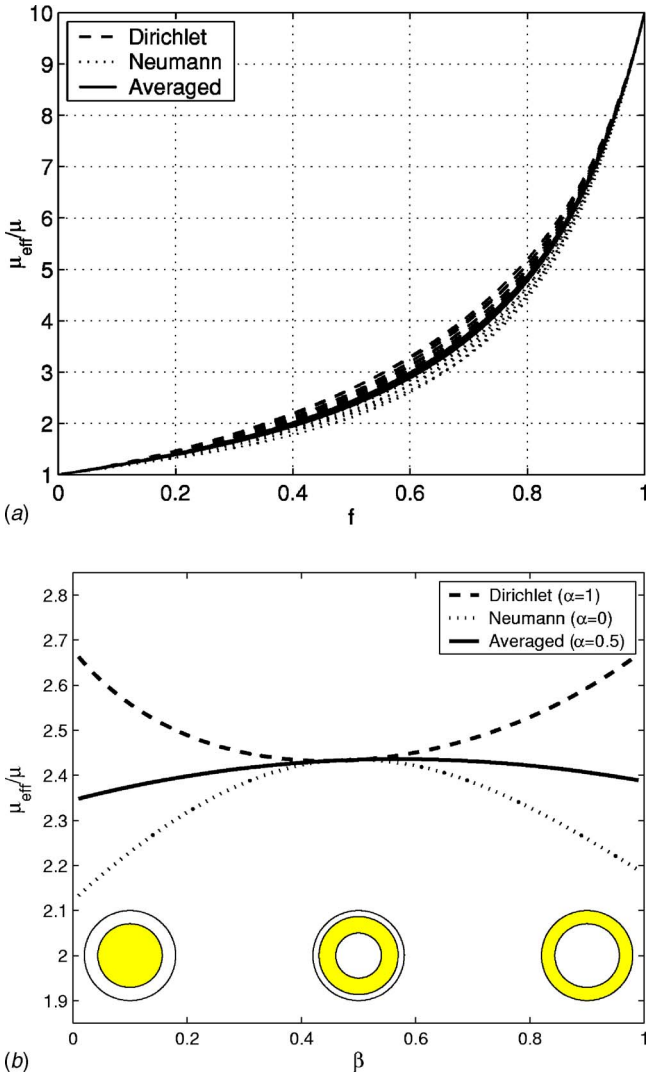

Fig. 8 Influence of β on the effective shear modulus

6 New Variational Bounds

One of the useful homogenization methods for composite materials are the Hashin–Shtrikman variational principles, which have been extensively used in deriving bounds for effective material properties. In the procedure of deriving the variational bounds, the Eshelby tensor is needed in order to estimate the disturbance strain field due to stress polarization or to estimate the disturbance stress field due to the eigenstrain.

Since the classical Eshelby tensor is obtained for an inclusion solution in an unbounded region, in principle, it can not be directly used in the derivation of the variational bounds of a composite with finite volume. In the past, additional probability arguments and approximations based on assumptions of the statistical nature of the inclusion distribution, have been employed to justify the use of the classical Eshelby tensor, e.g., Ref. [14].

In this section, we show that the finite Eshelby tensors are a perfect fit for the Hashin–Shtrikman variational principles [15,16]. They can be directly used in combination with the Hashin–Shtrikman principles to derive variational bounds without resorting to additional statistical arguments. By using the shell model proposed in the previous section, a systematic, multivariable optimization procedure is developed for multiphase composites.

We consider the case that the finite spherical RVE is subjected to a displacement boundary condition, i.e.

$$\mathbf{u}(\mathbf{x}) = \boldsymbol{\epsilon}^0\mathbf{x}, \quad \forall\, \mathbf{x}\in\partial\Omega \quad (106)$$

The standard statement of the Hashin–Shtrikman principles may be expressed in the following form

$$\underline{I}_p(\mathbf{p},\boldsymbol{\epsilon}^d) \leqslant \inf_{\boldsymbol{\epsilon}^d \in E} W(\boldsymbol{\epsilon}^d) \leqslant \bar{I}_p(\mathbf{p},\boldsymbol{\epsilon}^d) \tag{107}$$

where

$$W(\boldsymbol{\epsilon}) = \frac{1}{2|\Omega|}\int_\Omega \boldsymbol{\sigma}:\boldsymbol{\epsilon}\, d\Omega \tag{108}$$

is the strain energy density, and

$$I_p(\mathbf{p},\boldsymbol{\epsilon}^d) = W_0(\boldsymbol{\epsilon}^0) - \frac{1}{2|\Omega|}\int_\Omega \{\mathbf{p}:(\mathbb{C}-\mathbb{C}_0)^{-1}:\mathbf{p} - \mathbf{p}:\boldsymbol{\epsilon}^d - 2\mathbf{p}:\boldsymbol{\epsilon}^0\} d\Omega \tag{109}$$

Here $\mathbb{C}$ is the elastic tensor of the composite and $\mathbb{C}_0$ is the elastic tensor of a comparison solid such that

$$I_p = \begin{cases} \bar{I}_p, & \text{if } \Delta\mathbb{C} = \mathbb{C} - \mathbb{C}_0 < 0 \\ \underline{I}_p, & \text{if } \Delta\mathbb{C} = \mathbb{C} - \mathbb{C}_0 > 0 \end{cases} \tag{110}$$

Here $W_0(\boldsymbol{\epsilon}^0)$ is the strain energy density of the comparison solid; $\mathbf{p}$ is the stress polarization; and $\boldsymbol{\epsilon}^d$ is the disturbance strain field due to the stress polarization. They are related by the following subsidiary boundary value problem

$$\nabla\cdot[\mathbb{C}_0:\nabla\mathbf{u}^d(\mathbf{x}) + \mathbf{p}(\mathbf{x})] = 0, \quad \forall\, \mathbf{x} \in \Omega, \quad \mathbf{u}^d(\mathbf{x}) = 0, \quad \forall\, \mathbf{x} \in \partial\Omega \tag{111}$$

We consider the composite to be made of n distinct phases and assume that each phase may be represented by a hollow spherical shell inside the RVE. The homogenization or statistical model of the composite is that any macropoint of the composite is modeled as a RVE consisting of n distinct concentric spherical shells with domain Ω_i so that $\cup_i^n \Omega_i = \Omega$ and $\cap_{i=1}^n \Omega_i = \emptyset$. The stress polarization is chosen as a piecewise constant tensorial field

$$\mathbf{p}(\mathbf{x}) = \sum_{i=1}^n \mathbf{p}_i \chi(\Omega_i)$$

with

$$\chi(\Omega_i) = \begin{cases} 1, & \forall \mathbf{x} \in \Omega_i \\ 0, & \forall \mathbf{x} \notin \Omega_i \end{cases} \tag{112}$$

Let us consider

$$\mathbf{p}_i = p_i \mathbb{I}^{(2)} + \tau_i \mathbb{J}^{(2)} \tag{113}$$

where $\mathbb{I}^{(2)}$ is the second-order unit tensor and $\mathbb{J}^{(2)}$ is its counterpart, the so-called deviatoric unit tensor, both defined as

$$\mathbb{I}^{(2)} = \delta_{ij}\mathbf{e}_i \otimes \mathbf{e}_j, \quad \delta_{ij} = \begin{cases} 1, & i = j \\ 0, & i \neq j \end{cases},$$

$$\mathbb{J}^{(2)} = \beta_{ij}\mathbf{e}_i \otimes \mathbf{e}_j, \quad \beta_{ij} = \begin{cases} 0, & i = j \\ 1, & i \neq j \end{cases} \tag{114}$$

Based on the finite spherical inclusion model, the average disturbance strain will be the summation of the average disturbance strain in each phase

$$\langle \boldsymbol{\epsilon}^d \rangle_\Omega = -\sum_{i=1}^n \sum_{j=1}^n \mathbb{C}_0^{-1}:\langle \mathbb{S}^{ij,D} \rangle : \mathbf{p}_i \tag{115}$$

As shown in Sec. 2, the average Eshelby tensor can be written as

$$\langle \mathbb{S}^{ij,D} \rangle = s_1^{ij,D}\mathbb{E}^{(1)} + s_2^{ij,D}\mathbb{E}^{(2)} \tag{116}$$

We choose the prescribed boundary field as

$$\boldsymbol{\epsilon}^0 = \bar{\epsilon}\mathbb{I}^{(2)} + \bar{\gamma}\mathbb{J}^{(2)} \tag{117}$$

so that we obtain

$$\begin{aligned} I_p &= W_0(\bar{\boldsymbol{\epsilon}}) - \frac{1}{2|\Omega|}\int_\Omega \{\mathbf{p}:(\mathbb{C}-\mathbb{C}_0)^{-1}:\mathbf{p} - \mathbf{p}:\boldsymbol{\epsilon}^d - 2\mathbf{p}:\bar{\boldsymbol{\epsilon}}\} d\Omega \\ &= \frac{9}{2}\kappa_0\bar{\epsilon}^2 + 6\mu_0\bar{\gamma}^2 - \sum_{i=1}^n \left[\frac{f_i p_i^2}{2(\kappa_i - \kappa_0)} + \frac{3f_i\tau_i^2}{2(\mu_i - \mu_0)}\right] \\ &\quad - \sum_{i=1}^n \sum_{j=1}^n \left(\frac{f_i s_1^{ji,D} p_i p_j}{2\kappa_0} + \frac{3f_i s_2^{ji,D}\tau_i\tau_j}{2\mu_0}\right) + \sum_{i=1}^n (3f_i p_i\bar{\epsilon} + 6f_i\tau_i\bar{\gamma}) \end{aligned} \tag{118}$$

We first let $\partial I_p/\partial p_i = 0$. One can thus find

$$-\frac{p_i}{\kappa_i - \kappa_0} - \frac{s_1^{ii,D}p_i}{\kappa_0} - \sum_{j\neq i}\frac{s_1^{ji,D}p_j}{2\kappa_0} + 3\bar{\epsilon} = 0, \quad \forall\, i = 1,2,\cdots n \tag{119}$$

Hence the stationary value of each p_i can be obtained through the following system of equations

$$\begin{bmatrix} \ddots & & & & & & \\ \cdots & \cdots & \left(\frac{s_1^{ii,D}}{\kappa_0} + \frac{1}{\kappa_i - \kappa_0}\right) & \cdots & \frac{s_1^{ji,D}}{2\kappa_0} & \cdots & \\ & & & \ddots & & & \\ & & & & \ddots & & \\ & & & & & \ddots & \end{bmatrix} \begin{bmatrix} p_1 \\ \vdots \\ p_i \\ \vdots \\ p_j \\ \vdots \\ p_n \end{bmatrix} = 3\bar{\epsilon} \begin{bmatrix} 1 \\ \vdots \\ \vdots \\ 1 \\ \vdots \\ \vdots \\ 1 \end{bmatrix} \tag{120}$$

We further let $\partial I_p/\partial\tau_i = 0$, which leads to

$$-\frac{3f_i\tau_i}{\mu_i - \mu_0} - \frac{3f_i s_2^{ii,D}\tau_i}{\mu_0} - \sum_{j\neq i}\frac{3f_i s_2^{ji,D}\tau_j}{2\mu_0} + 6f_i\bar{\gamma} = 0 \tag{121}$$

or in matrix form

$$\begin{bmatrix} \ddots & & & & & & \\ \cdots & \cdots & \left(\frac{s_2^{ii,D}}{\mu_0} + \frac{1}{\mu_i - \mu_0}\right) & \cdots & \frac{s_2^{ji,D}}{2\mu_0} & \cdots & \\ & & & \ddots & & & \\ & & & & \ddots & & \\ & & & & & \ddots & \end{bmatrix} \begin{bmatrix} \tau_1 \\ \vdots \\ \tau_i \\ \vdots \\ \tau_j \\ \vdots \\ \tau_n \end{bmatrix} = 2\bar{\gamma} \begin{bmatrix} 1 \\ \vdots \\ \vdots \\ 1 \\ \vdots \\ \vdots \\ 1 \end{bmatrix} \tag{122}$$

Remark 6.1. In the past, when deriving variational bounds for multiphase composites, the same infinite Eshelby tensor was used for all the phases (except the comparison phase) without discrimination. This procedure excludes the interactions among different phases at the outset. By applying the shell model, proposed in the last section, with the finite Eshelby tensor this interaction can now be taken into account.

6.1 Two-Phase Composites. We now consider an isotropic two-phase composite, with $\kappa_2 > \kappa_1$ and $\mu_2 > \mu_1$. For the effective bulk modulus, we find the following bound under the prescribed displacement boundary condition

$$\kappa_1 + \frac{f_2}{\frac{1}{\kappa_2 - \kappa_1} + \frac{s_1^{22,D}}{\kappa_1}} \leqslant \bar{\kappa} \leqslant \kappa_2 + \frac{f_1}{\frac{1}{\kappa_1 - \kappa_2} + \frac{s_1^{11,D}}{\kappa_2}} \tag{123}$$

where

$$s_1^{22,D} = \frac{(1+\nu_1)f_1}{3(1-\nu_1)}$$

and

$$s_1^{11,D} = \frac{(1+\nu_2)f_2}{3(1-\nu_2)} \tag{124}$$

A similar result can be derived for the Neumann boundary condition

$$\kappa_1^{-1} + \frac{f_2}{\dfrac{1}{\kappa_2^{-1}-\kappa_1^{-1}} + \dfrac{1-s_1^{22,N}}{\kappa_1^{-1}}} \geqslant \bar{\kappa}^{-1} \geqslant \kappa_2^{-1} + \frac{f_1}{\dfrac{1}{\kappa_1^{-1}-\kappa_2^{-1}} + \dfrac{1-s_1^{11,N}}{\kappa_2^{-1}}} \tag{125}$$

where

$$s_1^{22,N} = \frac{1+\nu_1+2(1-2\nu_1)f_2}{3(1-\nu_1)}$$

and

$$s_1^{11,N} = \frac{1+\nu_2+2(1-2\nu_2)f_1}{3(1-\nu_2)} \tag{126}$$

It can be shown, by algebraic manipulation, that the bounds (123) and (125) are identical. Furthermore, they are equal to the original Hashin–Strikman bounds, because the coefficients (124) and (126) are equal to those of the original infinite Eshelby tensor.

Similarly, the bounds for the shear modulus can be obtained as

$$\mu_1 + \frac{f_2}{\dfrac{1}{\mu_2-\mu_1} + \dfrac{s_2^{22,D}}{\mu_1}} \leqslant \bar{\mu} \leqslant \mu_2 + \frac{f_1}{\dfrac{1}{\mu_1-\mu_2} + \dfrac{s_2^{11,D}}{\mu_2}} \tag{127}$$

where

$$s_2^{22,D} = \frac{2(4-5\nu_1)f_1}{15(1-\nu_1)} - \frac{21f_2(1-f_2^{2/3})^2}{10(1-\nu_1)(7-10\nu_1)} \tag{128}$$

$$s_2^{11,D} = \frac{2(4-5\nu_2)f_2}{15(1-\nu_2)} - \frac{21f_1(1-f_1^{2/3})^2}{10(1-\nu_2)(7-10\nu_2)} \tag{129}$$

and

$$\mu_1^{-1} + \frac{f_2}{\dfrac{1}{\mu_2^{-1}-\mu_1^{-1}} + \dfrac{1-s_2^{22,N}}{\mu_1^{-1}}} \geqslant \bar{\mu}^{-1} \geqslant \mu_2^{-1} + \frac{f_1}{\dfrac{1}{\mu_1^{-1}-\mu_2^{-1}} + \dfrac{1-s_2^{11,N}}{\mu_2^{-1}}} \tag{130}$$

where

$$s_2^{22,N} = \frac{2(4-5\nu_1)+(7-5\nu_1)f_2}{15(1-\nu_1)} + \frac{84f_2^2(1-f_2^{2/3})^2}{10(1-\nu_1)(7+5\nu_1)} \tag{131}$$

$$s_2^{11,N} = \frac{2(4-5\nu_2)+(7-5\nu_2)f_1}{15(1-\nu_2)} + \frac{84f_1^2(1-f_1^{2/3})^2}{10(1-\nu_2)(7+5\nu_2)} \tag{132}$$

Now the shear modulus bounds (127) and (130), are distinct, and they are different from the original Hashin–Shtrikman bounds based on the classical Eshelby tensor in an unbounded RVE. The new variational bounds for both bulk and shear modulus are displayed in Fig. 9 with respect to f_2. The material data is chosen as $\kappa_2=4\kappa_1$, $\mu_2=10\mu_1$, and $\nu_1=0.3$ (implying $\nu_2=0.083$).

Figure 9(*a*) shows that the boundary conditions have no effect on the bulk modulus, whose bounds coincide with the original HS bounds. On the other hand the boundary conditions do affect the variational bounds of the shear modulus. In Fig. 9(*b*), the three sets of the variational bounds (Dirichlet, Neumann, and the original) for the shear modulus are juxtaposed in comparison. We note that the difference between these three pairs is solely caused by the second term in coefficients $s_2^{ii,D}$ and $s_2^{ii,N}$. Without the second term in Eqs. (128), (129), (131), and (132), the three sets of bounds will coincide.

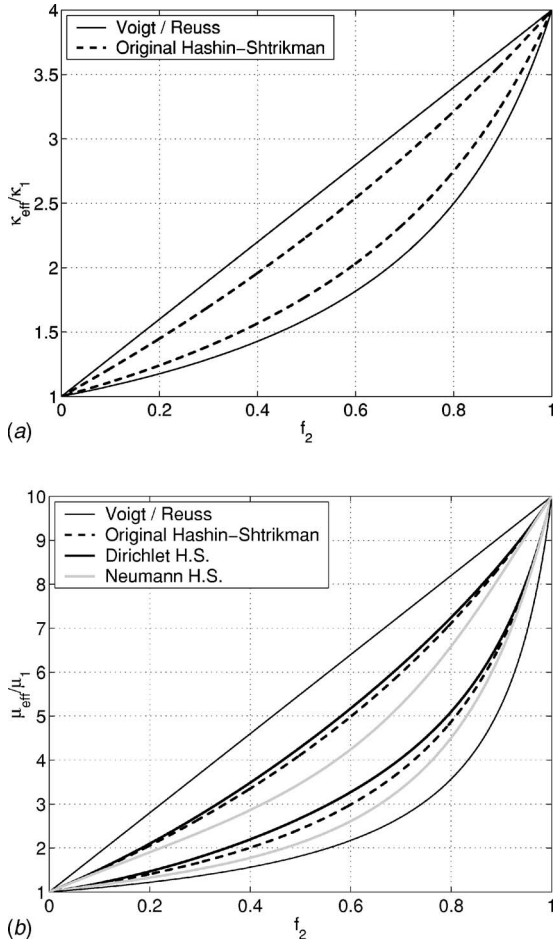

Fig. 9 Improved Hashin–Shtrikman bounds for the effective bulk and shear moduli

Remark 6.2. There is a difference between material ordering, i.e., $\kappa_1 \leqslant \kappa_2 \leqslant \cdots \leqslant \kappa_n$ and geometric ordering, i.e., concentric spherical shells $r_1 \leqslant r_2 \leqslant \cdots \leqslant r_n$. Since one does not necessarily place the phase with the smallest material constants in the inner most region of the RVE, the combination of mappings between material ordering and geometric ordering is multiple. There are differences in the homogenization results due to these different combinations.

For a two-phase composite, there are two ways to place the phase which is not the comparison phase in an RVE: either in the interior of the RVE or in the exterior of the RVE. By alternating the material phase from the interior region of the RVE to the exterior region of the RVE, the interior homogenization becomes the exterior homogenization, and they correspond to different finite Eshelby tensors as seen in Sec. 4. Therefore, in principle, we can obtain for each boundary condition two distinct pairs of the variational bounds, namely one corresponding to the interior eigenstrain and one corresponding to the exterior eigenstrain method (see Fig. 5 illustrating the different combinations possible for each boundary condition). For isotropic composites, alternating the phase position has no effect on the variational bounds for the bulk modulus, because the bulk part of the interior eigenstrain Eshelby tensor equals the bulk part of the exterior eigenstrain Eshelby tensor and thus the two pairs of bounds coincide.

On the other hand, for the shear modulus, alternating the phase position yields new variational bounds. (These are not shown in Fig. 9 since they will only deviate slightly from the bounds shown in the figure.) Altogether we have two pairs of distinct variational bounds for the shear modulus under each boundary condition.

For multiphase composites ($n \geqslant 3$), the dependence on phase position may become more pronounced.

6.2 Three-Phase Composites. Consider a three-phase isotropic composite with $\kappa_3 > \kappa_2 > \kappa_1$ and $\mu_3 > \mu_2 > \mu_1$. To obtain the lower bound, we choose $\kappa_0 = \kappa_1$ and $p_1 = 0$. One can then solve the stationarity condition Eq. (120) for p_2 and p_3

$$p_2 = 3\bar{\epsilon}\underline{p}_2, \quad \underline{p}_2 = \frac{1}{\Delta_{\ell 1}}\left(\frac{s_1^{33,D} - 0.5 s_1^{32,D}}{\kappa_1} + \frac{1}{\kappa_3 - \kappa_1}\right) \tag{133}$$

$$p_3 = 3\bar{\epsilon}\underline{p}_3, \quad \underline{p}_3 = \frac{1}{\Delta_{\ell 1}}\left(\frac{s_1^{22,D} - 0.5 s_1^{23,D}}{\kappa_1} + \frac{1}{\kappa_2 - \kappa_1}\right) \tag{134}$$

where

$$\Delta_{\ell 1} = \left(\frac{s_1^{22,D}}{\kappa_1} + \frac{1}{\kappa_2 - \kappa_1}\right)\left(\frac{s_1^{33,D}}{\kappa_1} + \frac{1}{\kappa_3 - \kappa_1}\right) - \frac{s_1^{32,D} s_1^{23,D}}{4\kappa_1^2} \tag{135}$$

Similarly, one can solve Eq. (120) for the stationary values of p_1 and p_2 for the upper bound by setting $\kappa_0 = \kappa_3$ and $p_3 = 0$, i.e.

$$p_1 = 3\bar{\epsilon}\bar{p}_1, \quad \bar{p}_1 = \frac{1}{\Delta_{u1}}\left(\frac{s_1^{22,D} - 0.5 s_1^{21,D}}{\kappa_3} + \frac{1}{\kappa_2 - \kappa_3}\right) \tag{136}$$

$$p_2 = 3\bar{\epsilon}\bar{p}_2, \quad \bar{p}_2 = \frac{1}{\Delta_{u1}}\left(\frac{s_1^{11,D} - 0.5 s_1^{12,D}}{\kappa_3} + \frac{1}{\kappa_1 - \kappa_3}\right) \tag{137}$$

where

$$\Delta_{u1} = \left(\frac{s_1^{11,D}}{\kappa_3} + \frac{1}{\kappa_1 - \kappa_3}\right)\left(\frac{s_1^{22,D}}{\kappa_3} + \frac{1}{\kappa_2 - \kappa_3}\right) - \frac{s_1^{12,D} s_1^{21,D}}{4\kappa_3^2} \tag{138}$$

Substituting the stationary values Eqs. (133), (134), (136), and (137), into the Hashin–Shtrikman variational principle Eq. (107), we find the explicit variational bounds of the bulk modulus for three-phase composites

$$\begin{aligned}\kappa_1 - \left[\frac{f_2 \underline{p}_2^2}{(\kappa_2 - \kappa_1)} + \frac{f_3 \underline{p}_3^2}{(\kappa_3 - \kappa_1)}\right] - \frac{1}{\kappa_1}(f_2 \underline{p}_2^2 s_1^{22,D} + f_2 \underline{p}_2 \underline{p}_3 s_1^{32,D} \\ + f_3 \underline{p}_2 \underline{p}_3 s_1^{23,D} + f_3 \underline{p}_3^2 s_1^{33,D}) + 2(f_2 \underline{p}_2 + f_3 \underline{p}_3) \leqslant \bar{\kappa} \leqslant \kappa_3 \\ - \left[\frac{f_1 \bar{p}_1^2}{(\kappa_1 - \kappa_3)} + \frac{f_2 \bar{p}_2^2}{(\kappa_2 - \kappa_3)}\right] - \frac{1}{\kappa_3}(f_1 \bar{p}_1^2 s_1^{11,D} + f_1 \bar{p}_1 \bar{p}_2 s_1^{21,D} \\ + f_2 \bar{p}_1 \bar{p}_2 s_1^{12,D} + f_2 \bar{p}_2^2 s_1^{22,D}) + 2(f_1 \bar{p}_1 + f_2 \bar{p}_2)\end{aligned} \tag{139}$$

Similarly, for the bounds of the shear modulus we have

$$\begin{aligned}\mu_1 - \left[\frac{f_2 \underline{\tau}_2^2}{(\mu_2 - \mu_1)} + \frac{f_3 \underline{\tau}_3^2}{(\mu_3 - \mu_1)}\right] - \frac{1}{\mu_1}(f_2 \underline{\tau}_2^2 s_2^{22,D} + f_2 \underline{\tau}_2 \underline{\tau}_3 s_2^{32,D} \\ + f_3 \underline{\tau}_2 \underline{\tau}_3 s_2^{23,D} + f_3 \underline{\tau}_3^2 s_2^{33,D}) + 2(f_2 \underline{\tau}_2 + f_3 \underline{\tau}_3) \leqslant \bar{\mu} \leqslant \mu_3 \\ - \left[\frac{f_1 \bar{\tau}_1^2}{(\mu_1 - \mu_3)} + \frac{f_2 \bar{\tau}_2^2}{(\mu_2 - \mu_3)}\right] - \frac{1}{\mu_3}(f_1 \bar{\tau}_1^2 s_2^{11,D} + f_1 \bar{\tau}_1 \bar{\tau}_2 s_2^{21,D} \\ + f_2 \bar{\tau}_1 \bar{\tau}_2 s_2^{12,D} + f_2 \bar{\tau}_2^2 s_2^{22,D}) + 2(f_1 \bar{\tau}_1 + f_2 \bar{\tau}_2)\end{aligned} \tag{140}$$

where

$$\underline{\tau}_2 = \frac{1}{\Delta_{\ell 2}}\left(\frac{s_2^{33,D} - 0.5 s_2^{32,D}}{\mu_1} + \frac{1}{\mu_3 - \mu_1}\right) \tag{141}$$

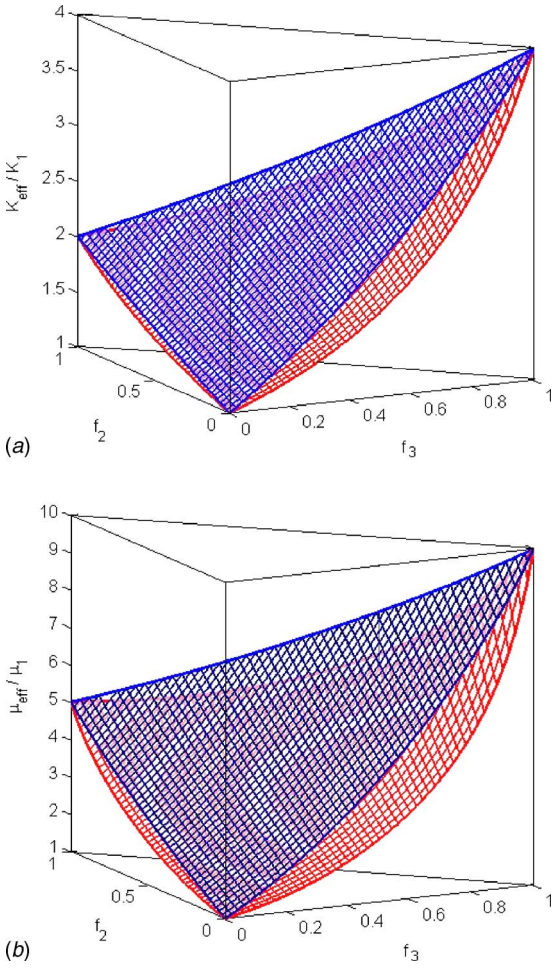

Fig. 10 Variational bounds for a three-phase composite material: (*a*) bounds for bulk modulus; and (*b*) bounds for shear modulus.

$$\underline{\tau}_3 = \frac{1}{\Delta_{\ell 2}}\left(\frac{s_2^{22,D} - 0.5 s_2^{23,D}}{\mu_1} + \frac{1}{\mu_2 - \mu_1}\right) \tag{142}$$

$$\bar{\tau}_1 = \frac{1}{\Delta_{u2}}\left(\frac{s_2^{22,D} - 0.5 s_2^{21,D}}{\mu_3} + \frac{1}{\mu_2 - \mu_3}\right) \tag{143}$$

$$\bar{\tau}_2 = \frac{1}{\Delta_{u2}}\left(\frac{s_2^{11,D} - 0.5 s_2^{12,D}}{\mu_3} + \frac{1}{\mu_1 - \mu_3}\right) \tag{144}$$

and

$$\Delta_{\ell 2} = \left(\frac{s_2^{22,D}}{\mu_1} + \frac{1}{\mu_2 - \mu_1}\right)\left(\frac{s_2^{33,D}}{\mu_1} + \frac{1}{\mu_3 - \mu_1}\right) - \frac{s_2^{23,D} s_2^{32,D}}{4\mu_1^2} \tag{145}$$

$$\Delta_{u2} = \left(\frac{s_2^{11,D}}{\mu_3} + \frac{1}{\mu_1 - \mu_3}\right)\left(\frac{s_2^{22,D}}{\mu_3} + \frac{1}{\mu_2 - \mu_3}\right) - \frac{s_2^{12,D} s_2^{21,D}}{4\mu_3^2} \tag{146}$$

Figure 10 shows the variational bounds for the effective bulk and shear modulus of a three-phase composite using the modulus ratios $\kappa_3:\kappa_2:\kappa_1 = 4:2:1$, $\mu_3:\mu_2:\mu_1 = 10:5:1$ and Poisson's ratio $\nu_1 = 0.3$. The unique features of variational bounds (139) and (140) are: (1) the boundary conditions are accurately taken into account without resorting to any approximation and ad hoc arguments; (2) interaction among different phases, or in other words, the correlation among different phases are precisely taken into account by

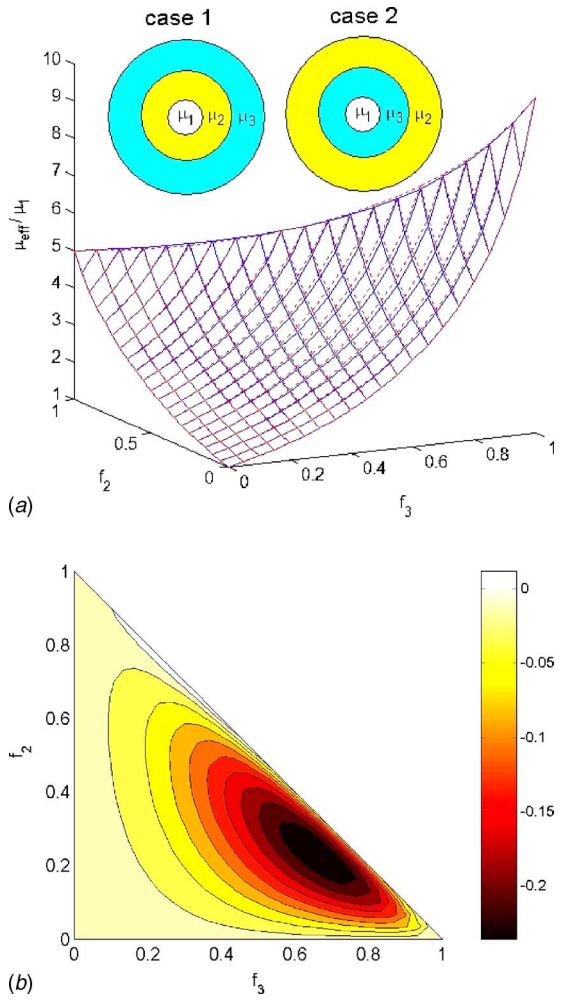

Fig. 11 Influence of phase position on three-phase variational bounds

the cross-term Eshelby tensor $S^{ij,D}$, $i \neq j$. This feature is absent in the classical HS bounds; (3) Microstructures of the composite are distinguished by mapping different combinations of the geometric ordering to the material ordering. For the bounds shown in Fig. 10, the geometric ordering coincides with the material ordering in ascending order, i.e., $(\kappa_1, \mu_1) \Rightarrow \Omega_1$, $(\kappa_2, \mu_2) \Rightarrow \Omega_2$, and $(\kappa_3, \mu_3) \Rightarrow \Omega_3$.

To examine the effect of the microstructure on the variational bounds, we exchange the material ordering within the domains Ω_2 and Ω_3. Figure 11(*a*) shows a plot of the two lower bound surfaces of the shear modulus. The contour of the difference is shown in Fig. 11(*b*). One can see that the maximum difference is about 0.2, demonstrating the the material ordering has little impact for this case.

7 Closure

In this paper, the finite Eshelby tensors obtained in Part I of our work are applied to develop various homogenization methods. It is shown that the special features of the finite Eshelby tensors can improve the accuracy of conventional homogenization methods and lead to more accurate predictions on effective material properties of composites.

For instance, we have found that for two-phase composites, there are at least two sets of Hashin–Shtrikman variational bounds corresponding to two different boundary conditions. This discovery may be instrumental for numerical homogenization procedures.

Furthermore, we have developed some new homogenization schemes such as the exterior eigenstrain method, dual eigenstrain method, i.e., a generalized self-consistency method, the shell model, and multiphase Hashin–Shtrikman bounds, which will enrich the engineering homogenization repertoire and provide sharper estimates on effective material properties of multi-phase composites.

The applications of the finite Eshelby tensor are multitude, and they are not limited to applications of homogenization theory. As indicated by the multilayer shell model, the finite Eshelby tensors provide the basic module to construct the multi-inclusion model and interface model, which can be used in modeling quantum dots, nano-onions, spinodal decomposition, and functionally graded materials. Some of these studies will be reported in separate papers.

Acknowledgment

This work is supported by a grant from National Science Foundation (Grant No. CMS-0239130), which is greatly appreciated.

Appendix: Table of the Eshelby Coefficients for the Three-Layer Shell Model

In this Appendix, a complete list of the coefficients for the average Eshelby tensors of a three-sphere RVE is documented. The notation of these coefficients is explained and defined in Sec. 5

$$s_1^{I1,D} = \frac{(1+\nu)(1-f_1)}{3(1-\nu)}$$

$$s_1^{I1,N} = \frac{(1+\nu)+2(1-2\nu)f_1}{3(1-\nu)}$$

$$s_2^{I1,D} = \frac{2(4-5\nu)(1-f_1)}{15(1-\nu)} - 21\gamma_u[f_1](1-f_1^{2/3})$$

$$s_2^{I1,N} = \frac{2(4-5\nu)+(7-5\nu)f_1}{15(1-\nu)} + 21\gamma_t[f_1](1-f_1^{2/3})$$

$$s_1^{I2,D} = -\frac{(1+\nu)f_1}{3(1-\nu)}$$

$$s_1^{I2,N} = \frac{2(1-2\nu)f_1}{3(1-\nu)}$$

$$s_2^{I2,D} = -\frac{2(4-5\nu)f_1}{15(1-\nu)} - 21\gamma_u[f_1]\left[1-\frac{(f_1+f_2)^{5/3}-f_1^{5/3}}{f_2}\right]$$

$$s_2^{I2,N} = \frac{(7-5\nu)f_1}{15(1-\nu)} + 21\gamma_t[f_1]\left[1-\frac{(f_1+f_2)^{5/3}-f_1^{5/3}}{f_2}\right]$$

$$s_1^{I3,D} = -\frac{(1+\nu)f_1}{3(1-\nu)}$$

$$s_1^{I3,N} = \frac{2(1-2\nu)f_1}{3(1-\nu)}$$

$$s_2^{I3,D} = -\frac{2(4-5\nu)f_1}{15(1-\nu)} + 21\gamma_u[f_1]\frac{(f_1+f_2)[1-(f_1+f_2)^{2/3}]}{f_3}$$

$$s_2^{I3,N} = \frac{(7-5\nu)f_1}{15(1-\nu)} - 21\gamma_t[f_1]\frac{(f_1+f_2)[1-(f_1+f_2)^{2/3}]}{f_3}$$

$$s_1^{II1,D} = \frac{(1+\nu)f_3}{3(1-\nu)}$$

$$s_1^{II1,N} = \frac{(1+\nu)+2(1-2\nu)(f_1+f_2)}{3(1-\nu)}$$

$$s_2^{II1,D} = \frac{2(4-5\nu)f_3}{15(1-\nu)} - 21\gamma_u(f_1+f_2)(1-f_1^{2/3})$$

$$s_2^{II1,N} = \frac{2(4-5\nu)+(7-5\nu)(f_1+f_2)}{15(1-\nu)} + 21\gamma_t(f_1+f_2)(1-f_1^{2/3})$$

$$s_1^{II2,D} = \frac{(1+\nu)f_3}{3(1-\nu)}$$

$$s_1^{II2,N} = \frac{(1+\nu)+2(1-2\nu)(f_1+f_2)}{3(1-\nu)}$$

$$s_2^{II2,D} = \frac{2(4-5\nu)}{15(1-\nu)}f_3 - 21\gamma_u(f_1+f_2)\left[1-\frac{(f_1+f_2)^{5/3}-f_1^{5/3}}{f_2}\right]$$

$$s_2^{II2,N} = \frac{2(4-5\nu)+(7-5\nu)(f_1+f_2)}{15(1-\nu)} + 21\gamma_t(f_1+f_2)\left[1-\frac{(f_1+f_2)^{5/3}-f_1^{5/3}}{f_2}\right]$$

$$s_1^{II3,D} = -\frac{(1+\nu)(f_1+f_2)}{3(1-\nu)}$$

$$s_1^{II3,N} = \frac{2(1-2\nu)(f_1+f_2)}{3(1-\nu)}$$

$$s_2^{II3,D} = -\frac{2(4-5\nu)}{15(1-\nu)}(f_1+f_2) + 21\gamma_u(f_1+f_2)\frac{(f_1+f_2)[1-(f_1+f_2)^{2/3}]}{f_3}$$

$$s_2^{II3,N} = \frac{7-5\nu}{15(1-\nu)}(f_1+f_2) - 21\gamma_t(f_1+f_2)\frac{(f_1+f_2)[1-(f_1+f_2)^{2/3}]}{f_3}$$

$$s_1^{III3,D} = 0$$

$$s_1^{III3,N} = 1$$

$$s_2^{III3,D} = 0$$

$$s_2^{III3,N} = 1$$

$$s_1^{III1,D} = 0$$

$$s_1^{III1,N} = 1$$

$$s_2^{III1,D} = 0$$

$$s_2^{III1,N} = 1$$

$$s_1^{III2,D} = 0$$

$$s_1^{III2,N} = 1$$

$$s_2^{III2,D} = 0$$

$$s_2^{III2,N} = 1$$

where

$$\gamma_u[x] := \frac{x(1-x^{2/3})}{10(1-\nu)(7-10\nu)}$$

and

$$\gamma_t[x] := \frac{4x(1-x^{2/3})}{10(1-\nu)(7+5\nu)} \tag{A1}$$

References

[1] Li, S., Sauer, R. A., and Wang, G., 2006, "The Eshelby Tensors in a Finite Spherical Domain—Part I: Theoretical Formulations," ASME J. Appl. Mech., **74**, pp. 770–783.

[2] Calvert, P., 1999, "Nanotube Composites: A Recipe for Strength," Nature (London), **399**, pp. 210–211.

[3] Thostenson, E. T., Ren, Z., and Chou, T. W., 2001, "Advances in Science and Technology of Carbon Nanotubes and Their Composites: A Review," Compos. Sci. Technol., **61**, pp. 1899–1912.

[4] Fisher, F. T., Bradshaw, R. D., and Brinson, L. C., 2002, "Effects of Nanotube Waviness on the Modulus of Nanotube-Reinforced Polymers," Appl. Phys. Lett., **80**, pp. 4647–4649.

[5] Odegard, G. M., Gates, T. S., Wise, K. E., Park, C., and Siochi, E. J., 2003, "Constitutive Modeling of Nanotube-Reinforced Polymer Composites," Compos. Sci. Technol., **63**, pp. 1671–1687.

[6] Shi, D.-L., Feng, X.-Q., Huang, Y.-Y., Hwang, K.-C., and Gao, H., 2004, "The Effect of Nanotube Waviness and Agglomeration on the Elastic Property of Carbon Nanotube-Reinforced Composites," J. Eng. Mater. Technol., **126**, pp. 250–257.

[7] Sharma, P., and Ganti, S., 2004, "Size-Dependent Eshelby's Tensor for Embedded Nano-Inclusions Incorporating Surface/Interface Energies," ASME J. Appl. Mech., **71**, pp. 663–671.

[8] Ovid'ko, I. A., and Scheinerman, A. G., 2005, "Elastic Fields of Inclusion in Nanocomposite Solids," Rev. Adv. Mater. Sci., **9**, pp. 17–33.

[9] Tanaka, K., and Mori, T., 1972, "Note on Volume Integrals of the Elastic Field Around an Ellipsoidal Inclusion," J. Elast., **2**, pp. 199–200.

[10] Nemat-Nasser, S., and Hori, M., 1999, *Micromechanics: Overall Properties of Heterogeneous Materials*, Elsevier, Amsterdam, The Netherlands.

[11] Mori, T., and Tanaka, K., 1973, "Average Stress in Matrix and Average Elastic Energy of Materials with Misfiting Inclusion," Acta Metall., **21**, pp. 571–574.

[12] Sauer, R. A., Wang, G., and Li, S., 2007, "The Composite Eshelby Tensors and Their Application to Homogenization," submitted.

[13] Castles, R. R., and Mura, T., 1985, "The Analysis of Eigenstrains Outside of an Ellipsoidal Inclusion," J. Elast., **15**, pp. 27–34.

[14] Willis, J. R., 1981, "Variational and Related Methods for the Overall Properties of Composites," *Advances in Applied Mechanics*, C. S. Vih, ed., Academic, New York, Vol. 21, pp. 1–78.

[15] Hashin, Z., and Shtrikman, S., 1962, "On Some Variational Principles in Anisotropic and Nonhomogeneous Elasticity," J. Mech. Phys. Solids, **10**, pp. 335–342.

[16] Hashin, Z., and Shtrikman, S., 1962, "A Variational Approach to the Theory of the Elastic Behavior of Polycrystals," J. Mech. Phys. Solids, **10**, pp. 343–352.